

Effective model and Magnetic Properties of the Resistive Electron Quadrupling State

Julien Garaud^{1,2,*} and Egor Babaev^{3,†}

¹*Institut Denis Poisson CNRS-UMR 7013, Université de Tours, 37200 Tours, France*

²*Nordita, Stockholm University, Roslagstullsbacken 23, SE-106 91 Stockholm, Sweden*

³*Department of Physics, KTH Royal Institute of Technology, SE-106 91 Stockholm, Sweden*

(Dated: August 18, 2022)

Recent experiments [V. Grinenko *et al.* *Nat. Phys.* **17**, 1254 (2021)] reported the observation of a condensate of four-fermion composites. This is a resistive state that spontaneously breaks the time-reversal symmetry, leading to unconventional magnetic properties, detected in muon spin rotation experiments and by the appearance of a spontaneous Nernst effect. In this work, we derive an effective model for the four-fermion order parameter that describes the observed spontaneous magnetic fields in this state. We show that this model, which is alike to the Faddeev-Skyrme model can host skyrmions: magnetic-flux-carrying topological excitations.

Recent experiments [1] reported the observation of a fermion quadrupling state in the multiband material: hole-doped $\text{Ba}_{1-x}\text{K}_x\text{Fe}_2\text{As}_2$. This resistive state, coined quartic bosonic metal, is a condensate with an anticorrelated flow of pairs of Cooper pairs belonging to different bands. In contrast to superconductors, which break the $U(1)$ gauge symmetry, this state spontaneously breaks the two-fold (\mathbb{Z}_2) time-reversal symmetry. This raises the question of the properties of such states.

An effective model can describe the properties of condensates at large length scales. For a pair condensate, the effective model is the celebrated Ginzburg-Landau theory which has been extensively studied since the second half of the last century. The question of effective models describing the fermion quadruplet quartic metal is more subtle. In this paper, we derive an effective long-wavelength model for the resistive quartic state reported in $\text{Ba}_{1-x}\text{K}_x\text{Fe}_2\text{As}_2$. Based on this, we report the key properties of that state: Namely its magnetic properties and the nature of the topological excitations it supports.

At low temperatures, the compound is a superconductor characterized by Cooper pair condensates Δ_a , forming in the different bands labeled by a . Importantly this superconductor breaks the time-reversal symmetry [2, 3], so that the total symmetry broken by the low-temperature state is $U(1) \times \mathbb{Z}_2$. The analysis of the magnitude and polarization of spontaneous magnetic fields [3–5] indicates a spin-singlet superconducting state that breaks the time-reversal symmetry. It is the so-called $s+is$ state which has two energetically equivalent locking of the relative phase $\theta_b - \theta_a$ between the superconducting gaps in different components $\Delta_{a,b}$.

The mechanism responsible for the appearance of the quartic metal is the following: The standard assumption of the Bardeen-Cooper-Schrieffer theory is a mean-field approximation for the fields quadratic in fermions: This assumption eliminates, by construction, the possibility for fermion quadrupling. The resulting theory yields the phase diagram of such a superconductor, which is typically a dome of the $s+is$ state between two different superconducting states [6–10]. It was pointed out in [11, 12], that relaxing the mean-field approximation

in a multicomponent fermion pairing theory results in a phase diagram with the appearance of fermion quadrupling condensates. The large-scale Monte Carlo calculations of $U(1) \times \mathbb{Z}_2$ states demonstrated that the discrete \mathbb{Z}_2 transition can exceed the superconducting $U(1)$ transition: $T_c < T_c^{\mathbb{Z}_2}$ [13–15].

The spontaneous breakdown of the time-reversal symmetry in the resistive state of $\text{Ba}_{1-x}\text{K}_x\text{Fe}_2\text{As}_2$, at the doping level $x \approx 0.8$ [1] dictates that the averages of the pairing order parameters Δ_a are zero, but that there exists a nonzero order parameter which is fourth order in the fermionic fields. The quadrupling order parameter is proportional to the product of pairing order parameters in different bands $\Delta_a^* \Delta_b$. Such an order parameter implies an anticorrelation in the flows of the components a and b . Crucially, although these types of counterflows do not represent superconductivity, they are generally coupled to the magnetic field when the densities of the counterflowing charged components are unequal. An effective model should account for this coupling, and should be different from the Ginzburg-Landau model of a Meissner state.

Below we derive such an *effective* theory, based on the mean-field approximation for the four-fermion order parameter. We demonstrate that, in an inhomogeneous sample, the model supports spontaneous magnetic fields, consistently with the experimental results [1]. It also predicts the existence of topological excitations carrying a quantized magnetic flux, in the form of skyrmions.

We derive our effective model for a state with composite order, from a generic model of a superconductor with a two-component order parameter Ψ , with $\Psi^\dagger := (\psi_1^*, \psi_2^*)$. The detailed derivation from the microscopic theory can be found in Supplemental Material [16]. The generic Ginzburg-Landau free-energy density for a two-component superconductor reads as

$$\mathcal{F}(\Psi, \mathbf{A}) = \frac{\mathbf{B}^2}{2} + \frac{k_{ab,ij}}{2} (D_i \psi_a)^* D_j \psi_b + V(\Psi^\dagger, \Psi), \quad (1)$$

where $V(\Psi^\dagger, \Psi)$ is the potential energy term. The repeated indices are implicitly summed over, and the indices i, j denote the spatial coordinates while a, b label

the different components. The individual condensates are coupled to the vector potential \mathbf{A} , of the magnetic field $\mathbf{B} = \nabla \times \mathbf{A}$, via the gauge derivative $\mathbf{D} = \nabla + ie\mathbf{A}$ in the kinetic term. In this work, we focus on two-component models that break multiple symmetries. The symmetry breaking is encoded in the potential term $V(\Psi^\dagger, \Psi)$ which explicitly reduces the global SU(2) symmetry of a doublet of complex order parameters down to a smaller symmetry group. For example, the SU(2) symmetry is broken down to $U(1) \times \mathbb{Z}_2$, for a superconductor that breaks time-reversal symmetry such as $s+is$, $s+id$, $d+ig$, $p+ip$, or down to $U(1) \times \mathbb{Z}_3$ symmetry as was suggested for some nematic superconductors [17]. The composite order of interest arises if the fluctuations-driven restoration of the local gauge symmetry occurs without restoring the other broken symmetries. The existence of a composite order was demonstrated in systems featuring $U(1) \times U(1)$ [11, 12] and SU(2) [18, 19] symmetries and from these calculations it follows that composite order also exists for $U(1) \times \mathbb{Z}_n$ symmetries. While most of our results qualitatively apply to all of the above mentioned pairing mechanisms, we focus below on the case of the broken time-reversal symmetry $U(1) \times \mathbb{Z}_2$, and in particular on the $s+is$ state, motivated by the experiment on $\text{Ba}_{1-x}\text{K}_x\text{Fe}_2\text{As}_2$ [1]. Other related states with composite order were discussed in [20–29].

At the microscopic level, the minimal model features three distinct superconducting gaps $\Delta_{1,2,3}$ in three different bands, and the pairing that leads to the time-reversal symmetry breaking states is dominated by the competition between different interband repulsion channels [6, 8, 10]. In the case of an interband-dominated repulsive pairing, only two fields $\psi_{1,2}$ appear in the effective Ginzburg-Landau model for the superconducting state, see *e.g.* [8, 30, 31]. When starting from the microscopic three-band model, the relevant two-component Ginzburg-Landau theory features mixed-gradient terms, which can be eliminated by a linear transformation to new fields see *e.g.* [31, 32], and the Supplemental Material [16]. The resulting Ginzburg-Landau theory is characterized by the free-energy $F/F_0 = \int \mathcal{F}$ whose density reads as

$$\mathcal{F}(\Psi, \mathbf{A}) = \frac{\mathbf{B}^2}{2} + \frac{1}{2} |\mathbf{D}\Psi|^2 + V(\Psi^\dagger, \Psi). \quad (2)$$

To account for the four-fermion state, the Ginzburg-Landau theory (2) is first mapped onto a model that couples the supercurrent $\mathbf{J} = e\text{Im}(\Psi^\dagger \mathbf{D}\Psi)$ to a real 3-vector \mathbf{m} . It is defined as the projection of the superconducting degrees of freedom Ψ onto spin-1/2 Pauli matrices $\boldsymbol{\sigma}$: $\mathbf{m} = \Psi^\dagger \boldsymbol{\sigma} \Psi$; hence this is an order parameter which is fourth order in the fermionic fields. This order parameter depends on the relative phase between the original complex fields, and does not depend on the superconducting degree of freedom: the phase sum. The norm of \mathbf{m} is related to the total density squared $\|\mathbf{m}\| \equiv \rho^2 = \Psi^\dagger \Psi$.

In terms of \mathbf{J} and \mathbf{m} , the free energy reads as [16]

$$\mathcal{F} = \frac{1}{2} \left[\epsilon_{kij} \left\{ \nabla_i \left(\frac{\mathbf{J}_j}{e^2 \rho^2} \right) - \frac{1}{4e\rho^6} \mathbf{m} \cdot \partial_i \mathbf{m} \times \partial_j \mathbf{m} \right\} \right]^2 + \frac{\mathbf{J}^2}{2e^2 \rho^2} + \frac{1}{8\rho^2} (\nabla \mathbf{m})^2 + V(\mathbf{m}), \quad (3)$$

where ϵ is the rank-3 Levi-Civita symbol. The term in the square brackets in (3) is the magnetic field expressed through gradients of the matter fields. The first term there, is the contribution of the Meissner current \mathbf{J} to the magnetic field, while the second term accounts for the interband counterflow [33, 34]:

$$\mathbf{B} = \nabla \times \left(\frac{\mathbf{J}}{e^2 \rho^2} \right) - \frac{\epsilon_{abc}}{4e\rho^6} m_a \nabla m_b \times \nabla m_c. \quad (4)$$

The second term is particularly important: It is related to the counterflow of two components, since it has a form of gradients of the composite field $\psi_a^* \psi_b$, *i.e.* it depends on gradients of the relative phase between components. A counterflow of two identical charged components results in no charge transfer and hence does not couple to the magnetic field. However, if the densities of the components are locally imbalanced, the charge transport occurs. Thus the coupling to the magnetic field involves a dependence of the relative density gradients.

Next, the low-temperature model (3), which microscopic derivation is given in the Supplemental Material [16], is used to obtain an effective model of the fermion quadrupling phase. The fermion quadrupling phase identified in [1, 13, 14] is resistive. This is caused by the disorder of the superconducting phase due to the proliferation of topological defects. The effective model of the resulting fermion quadrupling state is obtained by removing the superconducting degrees of freedom from (3). Indeed, as demonstrated in Monte Carlo calculations, their prefactors are renormalized to zero [1, 13, 14, 18, 19, 22, 35–37]. It follows that the Meissner current vanishes ($\mathbf{J} = 0$), while the currents associated with gradients of the fermion quadrupling order parameter \mathbf{m} do not. Assuming that the critical temperatures of the \mathbb{Z}_2 and U(1) transitions are well separated, the free energy of the fermion quadrupling state can be written as

$$\mathcal{F}(\mathbf{m}) = \frac{(\mathbf{m} \cdot \partial_i \mathbf{m} \times \partial_j \mathbf{m})^2}{16e^2 \|\mathbf{m}\|^6} + \frac{(\nabla \mathbf{m})^2}{8 \|\mathbf{m}\|} + V(\mathbf{m}), \quad (5a)$$

$$\text{where } V(\mathbf{m}) = \sum_{a=0,x,y,z} \alpha_a^m m_a + \frac{1}{2} \sum_{a,b=0,x,y,z} \beta_{ab}^m m_a m_b. \quad (5b)$$

Here the component m_0 stands for the magnitude of \mathbf{m} , $m_0 := \|\mathbf{m}\|$ (see details of the microscopic expressions for the coefficients in [16]). The first term in (5) has to be retained because it depends only on the relative phases and densities of the original superconducting fields. Hence it cannot vanish at superconducting phase transition, when $T_c < T_c^{\mathbb{Z}_2}$ [38]. The fermion quadrupling

phase reported in [1] breaks the time-reversal symmetry. Hence the potential term (5b) breaks the symmetry associated with the vector \mathbf{m} down to \mathbb{Z}_2 . In the original Ginzburg-Landau model (2), the time-reversal operation is the complex conjugation of the superconducting condensates Ψ . Correspondingly, for the soft modulus vector it is a reflection of \mathbf{m} on the xz plane of the target space:

$$\mathcal{T}(\Psi) = \Psi^* \Leftrightarrow \mathcal{T}(\mathbf{m}) = (m_x, -m_y, m_z). \quad (6)$$

This means that the states that break the time-reversal symmetry must have $m_y \neq 0$. This is, for example, enforced by $\beta_{xx}^{\mathbf{m}} > 0$, since it penalizes m_x^2 . The other details of the analysis of the potential can be found in the Supplemental Material [16]. The essential features can be qualitatively summarized as follows: First, all of the coefficients involving a y index vanish: $\alpha_y^{\mathbf{m}} = \beta_{ay}^{\mathbf{m}} = \beta_{ya}^{\mathbf{m}} = 0$. Moreover, the criterion for the condensation is $\alpha_0^{\mathbf{m}^2} < \alpha_x^{\mathbf{m}^2} + \alpha_z^{\mathbf{m}^2}$, and also $\beta_{00}^{\mathbf{m}}, \beta_{zz}^{\mathbf{m}} > 0$.

The quadrupling phase appears when the mean-field approximation for the pairing fields is relaxed. The model (5) can be viewed as a mean-field approximation for the fermion quadrupling fields in a resistive state; such as the \mathbb{Z}_2 -metal reported in [1]. Since superconducting currents are absent in the resistive state, the magnetic field caused by the gradients in the fermion quadrupling fields becomes

$$\mathbf{B} = -\frac{\epsilon_{abc} m_a \nabla m_b \times \nabla m_c}{4e \|\mathbf{m}\|^3}. \quad (7)$$

In two spatial dimensions, the topological invariant, which is associated with the degree of the maps $\mathbf{m}/\|\mathbf{m}\| : \mathbb{S}^2 \mapsto \mathbb{S}_{\mathbf{m}}^2$, reads as

$$\mathcal{Q}(\mathbf{m}) = \frac{1}{4\pi} \int_{\mathbb{R}^2} \frac{\mathbf{m} \cdot \partial_x \mathbf{m} \times \partial_y \mathbf{m}}{\|\mathbf{m}\|^3} dx dy. \quad (8)$$

The integrand is obviously ill defined when $\|\mathbf{m}\| = 0$. However, whenever $\|\mathbf{m}\| \neq 0$, the corresponding configuration has an integer topological charge $\mathcal{Q}(\mathbf{m}) \in \mathbb{Z}$; this suggests that the model can host skyrmion topological excitations. Note that in three dimensions the model is characterized by another invariant, the Hopf invariant, which is associated with the maps $\mathbb{S}^3 \mapsto \mathbb{S}_{\mathbf{m}}^2$. This suggests the existence of hopfions, but it is beyond the scope of the current discussion.

The model describing the resistive fermion quadrupling state is alike to the Faddeev-Skyrme model [39]. This suggests that it could host nontrivial topological excitation such as skyrmions and hopfions. To investigate the properties of the topological defects of the effective model, the physical degrees of freedom \mathbf{m} are discretized within a finite-element formulation [40], and the free energy (5) is minimized using a nonlinear conjugate gradient algorithm. For details of the numerical procedure, see [16].

The experiments [1] reported spontaneous magnetic fields in the quartic metal state. In the $s+is$ superconducting state, spontaneous magnetic fields can arise due

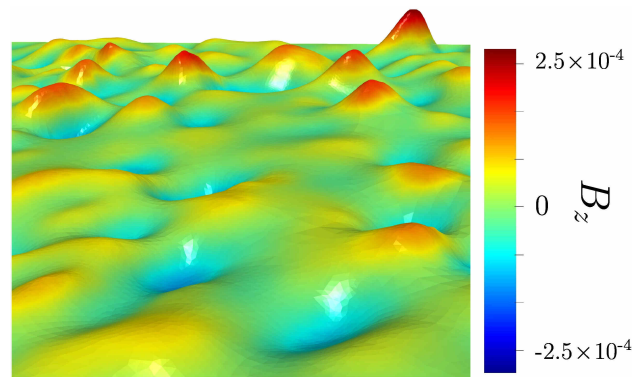


Figure 1. Spontaneous magnetic field \mathbf{B} (7) in the quartic phase, generated by inhomogeneities. The inhomogeneities are modeled by random spatial modulation of the parameters $\alpha_0^{\mathbf{m}}$ and $\alpha_z^{\mathbf{m}}$, reflecting the naturally present weak gradients in doping level. The surface elevation, together with the coloring, represents the magnitude of the B_z . The coupling here is $e = 0.6$, and the other parameters are given in Supplemental Material [16].

to inhomogeneities such as thermal gradients [1, 41], a hotspot created by a laser pulse [30], the effect of impurities [42, 43], and other inhomogeneous arrays [4, 32]. The material has slight inhomogeneity in doping level, which results in relatively small local modulation of the superconducting critical temperature [44]. Since for this topic the relative values of the gaps and phases strongly depend on doping, this can be modeled by spatial modulation of the prefactors of the quadratic terms of the Ginzburg-Landau theory. Implementing smoothly spatially varying amplitudes of the individual components, at the level of the effective model, can thus be modeled by small spatial variations of the coupling constants $\alpha_0^{\mathbf{m}}$ and $\alpha_z^{\mathbf{m}}$ (see Supplemental Material for details [16]). As shown in Fig. 1, such inhomogeneities in the effective model for the fermion quadrupling state, which breaks the time-reversal symmetry, result in spontaneous magnetic fields. It is qualitatively in accordance with the experiment [1].

First note that because the time-reversal symmetry (\mathbb{Z}_2) is broken, the model has domain-wall excitations. These are similar, in a way, to the domain walls found in a three-component model [1, 45]. They are thus discussed in the Supplemental Material [16]. However the quantization of $\mathcal{Q}(\mathbf{m})$ suggests that the model has more nontrivial topological excitations with quantized magnetic flux according to $\int B_z = \Phi_0 \mathcal{Q}$, where $\Phi_0 = -2\pi/e$ is the flux quantum. If a model breaks the \mathbb{Z}_2 symmetry and has only gradient terms which are second order in derivatives, according to the Hobart-Derrick theorem [46, 47], skyrmions cannot exist. In our case, the presence of the Skyrme term, in the effective model (5), allows for nontrivial configurations that evade the Hobart-Derrick theorem. Indeed, in two dimensions, the Skyrme term in the effective model scales as $1/R^2$ (where R is a texture size), and therefore stable skyrmions may exist due to the

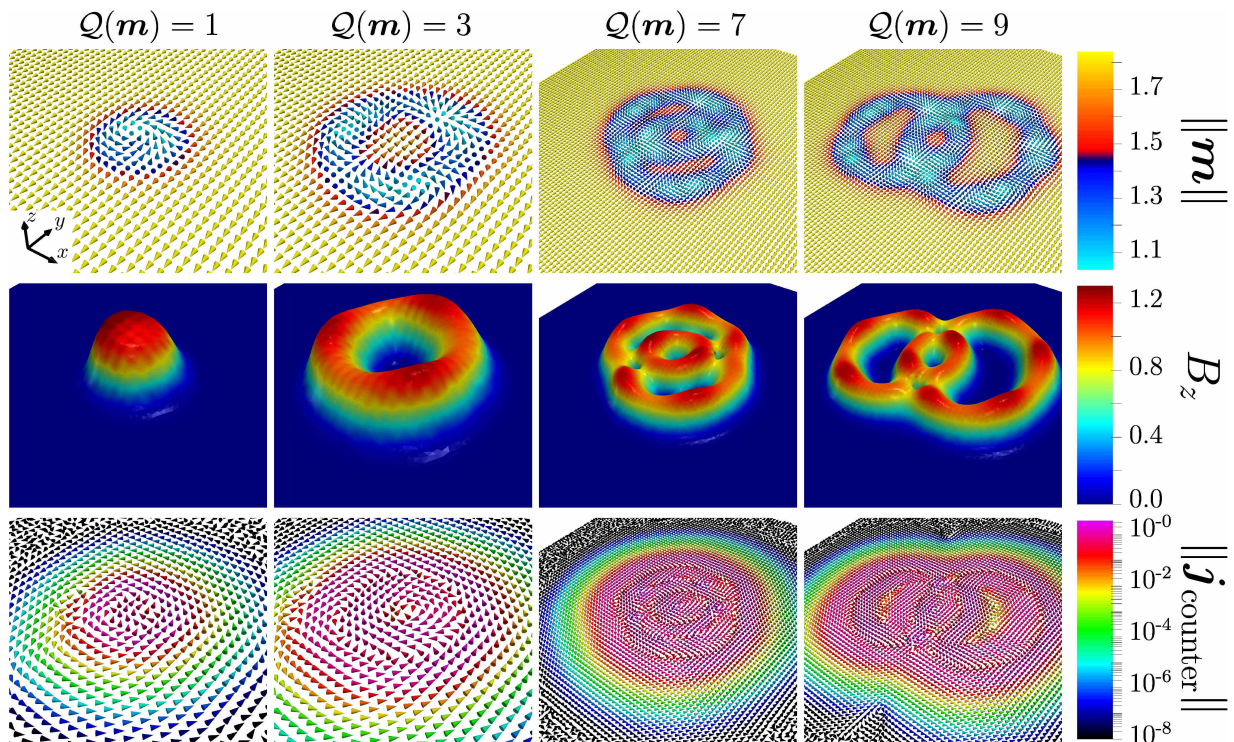


Figure 2. Skymion solutions in a time-reversal symmetry broken state, for increasing values of the topological charge $Q(\mathbf{m})$. The panels on the top row display the texture of the four-fermion order parameter \mathbf{m} . The panels in the middle row show the associated magnetic field \mathbf{B} (7), and the bottom row shows the corresponding charge transferring counter-currents $\mathbf{j}_{\text{counter}}$ according to Ampère’s law. The parameters are the same as in Fig. 1, while the coupling $e = 0.25$.

competition between the Skyrme and potential terms.

We performed numerical simulation by minimizing the energy (5) from various initial states. When the initial guess has a nontrivial topological charge, the minimization procedure leads, after convergence of the algorithm, to stable skymion configurations. Figure 2 shows these skymions solutions for increasing values of the topological charge $Q(\mathbf{m})$, which is integer with an accuracy around 10^{-4} . As shown on the middle row of Fig. 2, the skymions carry a nonzero magnetic field. Moreover, since the topological charge (8) is quantized, the skymions carry integer quanta of magnetic flux. The circulating current pattern that induces this magnetic field is illustrated in the bottom row. This current, defined according to Ampère’s law for the magnetic field (7) corresponds to the charge-carrying counterflow between the different components.

Furthermore we find that the interskymion forces are attractive. Hence, single quanta skymions attract each other to form skymions with higher topological charge. Thus in general one would not expect the formation of regular skymion lattices but rather skymion lumps formed by the competition between the attractive forces and pinning landscape. Interestingly, in a single quantum skymion, the time-reversed state is realized at a zero measure area inside the skymion. On the other hand, skymions carrying more than one quantum feature in-

ner regions of the time-reversed state. The enclosed area of the time-reversed state increases with the topological charge. This suggests that if the \mathbb{Z}_2 symmetry associated with the relative phase locking is strongly broken, the formation of skymions is strongly inhibited. Note that unlike in Fig. 1, the parameters for the skymions displayed in Fig. 2 are homogeneous, as we focus here on the detailed structure of the skymions. Inhomogeneities can however deform the skymions, although we find that they do not destroy skymions (see Supplemental Material [16]).

The recent experiment reported a fermion quadrupling phase in $\text{Ba}_{1-x}\text{K}_x\text{Fe}_2\text{As}_2$ [1]. In this resistive phase, there is no condensate of Cooper pairs, but a four-fermion condensate which breaks the \mathbb{Z}_2 time-reversal symmetry.

We derived an effective model of that resistive state, starting from a microscopic three-band model with dominant interband interaction for $\text{Ba}_{1-x}\text{K}_x\text{Fe}_2\text{As}_2$ and by implementing a mean-field approximation for the fields that are fourth order in fermions. The effective field theory has a structure similar to the Faddeev-Skyrme model, but for a soft modulus vector field that represents the fermion quadrupling order parameter. If spatial inhomogeneities are present the model accounts for spontaneous magnetic fields, consistently with the experimental observations [1]. We report that despite the lack of Meissner effect and the lack of conserved $U(1)$ topological charge,

the model has stable topological excitations in the form of skyrmions with conserved topological charge given by (8).

We would like to remind the reader that, similarly to skyrmions that appear in other contexts, such as magnetism, their existence also depends on factors that are beyond the effective long-wavelength field-theoretic model. Namely, in contrast to vortices, the skyrmionic topological charge is obtained through a surface integral. Consequently, if the terms that break the $O(3)$ symmetry are very strong, the localization of the skyrmionic topological charge can shrink down to scales where the effective theory is ill defined, thereby destroying the topological protection. When the effective field theory is applicable, the potential barrier preventing the collapse of a skyrmion in a film can be roughly estimated as follows: the condensation energy density (F_c) multiplied by the coherence volume $F_c \xi_{Z_2}^2 L$, where ξ_{Z_2} is the coherence length associated with the broken time-reversal symme-

try and L is the film thickness.

Finally, within the range of applicability of the effective theory, the skyrmions can be induced by taking advantage of the Kibble-Zurek mechanism [48, 49], by quenching the material through the Z_2 phase transition where the time-reversal symmetry is broken. We expect that skyrmions may also form by cooling through the phase transition with an applied *local* magnetic field induced through a system of coils.

ACKNOWLEDGMENTS

We thank Vadim Grinenko for discussions. The work was supported by the Swedish Research Council Grants 2016-06122, 2018-03659. The computations were performed on resources provided by the Swedish National Infrastructure for Computing (SNIC) at the National Supercomputer Center at Linköping, Sweden.

* garaud.phys@gmail.com

† babaev.egor@gmail.com

- [1] V. Grinenko, D. Weston, F. Caglieris, C. Wuttke, C. Hess, T. Gottschall, I. Maccari, D. Gorbunov, S. Zherlitsyn, J. Wosnizza, A. Rydh, K. Kihou, C.-H. Lee, R. Sarkar, S. Dengre, J. Garaud, A. Charnukha, R. Hühne, K. Nielsch, B. Büchner, H.-H. Klauss, and E. Babaev, “State with spontaneously broken time-reversal symmetry above the superconducting phase transition,” *Nature Physics* **17**, 1254–1259 (2021).
- [2] V. Grinenko, P. Materne, R. Sarkar, H. Luetkens, K. Kihou, C. H. Lee, S. Akhmadaliev, D. V. Efremov, S.-L. Drechsler, and H.-H. Klauss, “Superconductivity with broken time-reversal symmetry in ion-irradiated $Ba_{0.27}K_{0.73}Fe_2As_2$ single crystals,” *Physical Review B* **95**, 214511 (2017).
- [3] V. Grinenko, R. Sarkar, K. Kihou, C. H. Lee, I. Morozov, S. Aswartham, B. Büchner, P. Chekhonin, W. Skrotzki, K. Nenkov, R. Hühne, K. Nielsch, S. L. Drechsler, V. L. Vadimov, M. A. Silaev, P. A. Volkov, I. Eremin, H. Luetkens, and H.-H. Klauss, “Superconductivity with broken time-reversal symmetry inside a superconducting *s*-wave state,” *Nature Physics* **16**, 789–794 (2020).
- [4] V. L. Vadimov and M. A. Silaev, “Polarization of the spontaneous magnetic field and magnetic fluctuations in *s + is* anisotropic multiband superconductors,” *Physical Review B* **98**, 104504 (2018).
- [5] M. Speight, T. Winyard, A. Wormald, and E. Babaev, “Magnetic field behavior in *s + is* and *s + id* superconductors: Twisting of applied and spontaneous fields,” *Physical Review B* **104**, 174515 (2021).
- [6] V. Stanev and Z. Tešanović, “Three-band superconductivity and the order parameter that breaks time-reversal symmetry,” *Physical Review B* **81**, 134522 (2010).
- [7] J. Carlström, J. Garaud, and E. Babaev, “Length scales, collective modes, and type-1.5 regimes in three-band superconductors,” *Physical Review B* **84**, 134518 (2011).
- [8] S. Maiti and A. V. Chubukov, “*s + is* state with broken time-reversal symmetry in Fe-based superconductors,” *Physical Review B* **87**, 144511 (2013).
- [9] M. Silaev, J. Garaud, and E. Babaev, “Phase diagram of dirty two-band superconductors and observability of impurity-induced *s + is* state,” *Physical Review B* **95**, 024517 (2017).
- [10] J. Böker, P. A. Volkov, K. B. Efetov, and I. Eremin, “*s + is* superconductivity with incipient bands: Doping dependence and STM signatures,” *Physical Review B* **96**, 014517 (2017).
- [11] E. Babaev, A. Sudbø, and N. W. Ashcroft, “A superconductor to superfluid phase transition in liquid metallic hydrogen,” *Nature* **431**, 666–668 (2004).
- [12] E. Babaev, “Phase diagram of planar $U(1) \times U(1)$ superconductor: condensation of vortices with fractional flux and a superfluid state,” [arXiv:cond-mat/0201547v7](https://arxiv.org/abs/cond-mat/0201547v7) (2002).
- [13] T. A. Bojesen, E. Babaev, and A. Sudbø, “Time reversal symmetry breakdown in normal and superconducting states in frustrated three-band systems,” *Physical Review B* **88**, 220511(R) (2013).
- [14] T. A. Bojesen, E. Babaev, and A. Sudbø, “Phase transitions and anomalous normal state in superconductors with broken time-reversal symmetry,” *Physical Review B* **89**, 104509 (2014).
- [15] J. Carlström and E. Babaev, “Spontaneous breakdown of time-reversal symmetry induced by thermal fluctuations,” *Physical Review B* **91**, 140504(R) (2015).
- [16] See Supplemental Material given as an Appendix, for detailed derivation, additional results, and discussion of the numerical methods.
- [17] C.-W. Cho, J. Shen, J. Lyu, O. Atanov, Q. Chen, S. H. Lee, Y. S. Hor, D. J. Gawryluk, E. Pomjakushina, M. Bartkowiak, M. Hecker, J. Schmalian, and R. Lortz, “ Z_3 -vestigial nematic order due to superconducting fluctuations in the doped topological insulators $NbxBi_2Se_3$ and $Cu_xBi_2Se_3$,” *Nature Communications* **11**, 3056 (2020).
- [18] A. B. Kuklov, M. Matsumoto, N. V. Prokof’ev, B. V. Svistunov, and M. Troyer, “Deconfined Criticality:

- Generic First-Order Transition in the SU(2) Symmetry Case,” *Physical Review Letters* **101**, 050405 (2008).
- [19] E. V. Herland, Tr. A. Bojesen, E. Babaev, and A. Sudbø, “Phase structure and phase transitions in a three-dimensional SU(2) superconductor,” *Physical Review B* **87**, 134503 (2013).
- [20] D. F. Agterberg and H. Tsunetsugu, “Dislocations and vortices in pair-density-wave superconductors,” *Nature Physics* **4**, 639–642 (2008).
- [21] E. Berg, E. Fradkin, and S. A. Kivelson, “Charge-4e superconductivity from pair-density-wave order in certain high-temperature superconductors,” *Nature Physics* **5**, 830–833 (2009).
- [22] A. B. Kuklov, N. V. Proko’ev, B. V. Svistunov, and M. Troyer, “Deconfined criticality, runaway flow in the two-component scalar electrodynamics and weak first-order superfluid-solid transitions,” *Annals of Physics* **321**, 1602–1621 (2006), July 2006 Special Issue.
- [23] O. Erten, P.-Y. Chang, P. Coleman, and A. M. Tsvelik, “Skyrme Insulators: Insulators at the Brink of Superconductivity,” *Physical Review Letters* **119**, 057603 (2017).
- [24] V. Fleurov and A. Kuklov, “Cooperative phases and phase transitions of Bose condensed light in dye filled cavities,” *New Journal of Physics* **21**, 083009 (2019).
- [25] D. Shaffer, J. Wang, and L. H. Santos, “Theory of Hofstadter superconductors,” *Physical Review B* **104**, 184501 (2021).
- [26] F. L. Buessen, S. Sorn, I. Martin, and A. Paramekanti, “Nematic order driven by superconducting correlations,” *Annals of Physics* **435**, 168494 (2021).
- [27] Rafael M. Fernandes and Liang Fu, “Charge-4e Superconductivity from Multicomponent Nematic Pairing: Application to Twisted Bilayer Graphene,” *Physical Review Letters* **127**, 047001 (2021).
- [28] S. B. Chung and S. K. Kim, “Berezinskii-Kosterlitz-Thouless transition transport in spin-triplet superconductor,” *SciPost Physics Core* **5** (2022), 10.21468/scipostphyscore.5.1.003.
- [29] V. Drouin-Touchette, P. P. Orth, P. Coleman, P. Chandra, and T. C. Lubensky, “Emergent Potts Order in a Coupled Hexatic-Nematic XY model,” *Physical Review X* **12**, 011043 (2022).
- [30] J. Garaud, M. Silaev, and E. Babaev, “Thermoelectric Signatures of Time-Reversal Symmetry Breaking States in Multiband Superconductors,” *Physical Review Letters* **116**, 097002 (2016).
- [31] J. Garaud, M. Silaev, and E. Babaev, “Microscopically derived multi-component Ginzburg–Landau theories for $s + is$ superconducting state,” *Physica C: Superconductivity and its Applications* **533**, 63–73 (2017).
- [32] J. Garaud, A. Corticelli, M. Silaev, and E. Babaev, “Properties of dirty two-band superconductors with repulsive interband interaction: Normal modes, length scales, vortices, and magnetic response,” *Physical Review B* **98**, 014520 (2018).
- [33] E. Babaev, L. D. Faddeev, and A. J. Niemi, “Hidden symmetry and knot solitons in a charged two-condensate Bose system,” *Physical Review B* **65**, 100512(R) (2002).
- [34] J. Garaud, J. Carlström, E. Babaev, and M. Speight, “Chiral CP² skyrmions in three-band superconductors,” *Physical Review B* **87**, 014507 (2013).
- [35] E. Smørgrav, E. Babaev, J. Smiseth, and A. Sudbø, “Observation of a Metallic Superfluid in a Numerical Experiment,” *Physical Review Letters* **95**, 135301 (2005).
- [36] J. Smiseth, E. Smørgrav, E. Babaev, and A. Sudbø, “Field- and temperature-induced topological phase transitions in the three-dimensional N -component London superconductor,” *Physical Review B* **71**, 214509 (2005).
- [37] D. Weston and E. Babaev, “Composite order in SU(N) theories coupled to an Abelian gauge field,” *Physical Review B* **104**, 075116 (2021).
- [38] This is because the topological charge of composite, single-quantum superconducting vortex has a winding only in the phase sum. Hence it cannot restore order in the fields that depend only on the relative phases and relative densities.
- [39] L. D. Faddeev and A. J. Niemi, “Knots and particles,” *Nature* **387**, 58–61 (1997).
- [40] F. Hecht, “New development in freefem++,” *Journal of Numerical Mathematics* **20**, 251–265 (2012), See also FreeFEM software at <https://freefem.org/>.
- [41] M. Silaev, J. Garaud, and E. Babaev, “Unconventional thermoelectric effect in superconductors that break time-reversal symmetry,” *Physical Review B* **92**, 174510 (2015).
- [42] S. Maiti, M. Sigrist, and A. Chubukov, “Spontaneous currents in a superconductor with $s + is$ symmetry,” *Physical Review B* **91**, 161102(R) (2015).
- [43] S.-Z. Lin, S. Maiti, and A. Chubukov, “Distinguishing between $s + id$ and $s + is$ pairing symmetries in multiband superconductors through spontaneous magnetization pattern induced by a defect,” *Physical Review B* **94**, 064519 (2016).
- [44] Y. Iguchi and et. al, (2022), to be published.
- [45] J. Garaud and E. Babaev, “Domain Walls and Their Experimental Signatures in $s + is$ Superconductors,” *Physical Review Letters* **112**, 017003 (2014).
- [46] R. H. Hobart, “On the Instability of a Class of Unitary Field Models,” *Proceedings of the Physical Society* **82**, 201–203 (1963).
- [47] G. H. Derrick, “Comments on Nonlinear Wave Equations as Models for Elementary Particles,” *Journal of Mathematical Physics* **5**, 1252–1254 (1964).
- [48] T. W. B. Kibble, “Topology of Cosmic Domains and Strings,” *Journal of Physics A: Mathematical and General* **9**, 1387–1398 (1976).
- [49] W. H. Zurek, “Cosmological experiments in superfluid helium?” *Nature* **317**, 505–508 (1985).

Supplemental Material: Skyrmions and magnetic properties of the resistive electron quadrupling state

In the Supplemental Material, we discuss the details of the derivation of the effective theory for the fermion quadrupling state. In particular, we start from the microscopic model of a three band superconductor with interband dominated pairing. This yields a two-component Ginzburg-Landau theory with inter-component mixed gradient terms which are then eliminated by a reparametrization of the superconducting degrees of freedom. Next, the theory is mapped to a model that couples the fermion quadrupling order parameter to the Meissner current. In the resistive state, the Meissner screening is absent, and the theory reduces to a model that depends only on the four-fermion order parameter. We also discuss details of the numerical methods, and present additional results. These include additional skyrmion solutions, the effect of material inhomogeneities on skyrmions, and domain-wall solutions.

I. MICROSCOPIC DERIVATION OF THE EFFECTIVE MODEL

The first part starts with the microscopic derivation of the two-component Ginzburg-Landau theory that is relevant to describe a three-band superconductor with interband dominated repulsive pairing. See [S1] for a more detailed derivation. We are interested in values of coupling constants that can result in superconducting states that spontaneously break the time-reversal symmetry, aiming in particular to describe iron pnictides. The band structure of iron pnictides typically consists of two electron pockets at $(0, \pi)$ and $(\pi, 0)$ and of two hole pockets at the Γ point. This structure is sketched on Fig. S1, where the dominating pairing channels are the interband repulsion between the two hole pockets at Γ , as well as between the electron and the hole bands. Note that, the order parameter is the same in both electron pockets, so that the crystalline C_4 symmetry is not broken and thus corresponds to an s -wave state.

A. Generic three-component expansion

We consider the microscopic model of a clean superconductor with three overlapping bands at the Fermi level. Within the quasiclassical approximation, the band parameters that characterize the different cylindrical sheets of the Fermi surface are the partial densities of states (DOS) ν_a , and the Fermi velocities $\mathbf{v}_F^{(a)}$; here the index $a = 1, 2, 3$ labels the different bands. The Eilenberger equations for the quasiclassical propagators read as

$$\hbar \mathbf{v}_F^{(a)} \mathbf{D} f_a + 2\omega_n f_a - 2\Delta_a g_a = 0, \quad (\text{S1a})$$

$$\hbar \mathbf{v}_F^{(a)} \mathbf{D}^* f_a^+ - 2\omega_n f_a^+ + 2\Delta_a^* g_a = 0, \quad (\text{S1b})$$

where $\omega_n = (2n + 1)\pi T$, with $n \in \mathbb{Z}$, are the fermionic Matsubara frequencies and T is the temperature. The gauge derivative is $\mathbf{D} \equiv \nabla + ie\mathbf{A}$, where \mathbf{A} is the vector potential, and the gauge coupling is related to the flux quantum Φ_0 by $e = -2\pi/\Phi_0$.

The quasi-classical propagators f_a and g_a are respectively, the anomalous and the normal Green's functions in each band; they obey the normalization condition

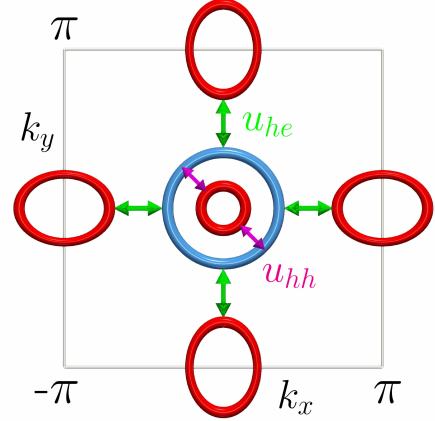


Figure S1. Schematic view of the band structure of the hole-doped iron pnictide compound $\text{Ba}_{1-x}\text{K}_x\text{Fe}_2\text{As}_2$. It consists of two hole pockets at the Γ point shown by circles and two electron pockets at $(0, \pi)$ and $(\pi, 0)$ displayed by ellipses. As discussed in the text, the $s+is$ state is favoured by the superconducting coupling that is dominated by the interband repulsion between the electron and the hole Fermi surfaces u_{he} , as well as between the two hole pockets u_{hh} .

$|f_a|^2 + g_a^2 = 1$. The components Δ_a of the order parameter are determined by the self-consistency equations

$$\Delta_a(\mathbf{p}, \mathbf{r}) = 2\pi T \sum_{n, \mathbf{p}', b} \lambda_{ab}(\mathbf{p}, \mathbf{p}') f_b(\mathbf{p}, \mathbf{r}, \omega_n). \quad (\text{S2})$$

Here, the parameters \mathbf{p} run over the Fermi surfaces, and λ_{ab} are the components of the coupling potential matrix. For simplicity the pairing states are assumed to be isotropic on each of the Fermi surfaces, so that $\lambda_{ab}(\mathbf{p}, \mathbf{p}') = \text{const}$, see details in [S1]. Finally, the self-consistent electric current is

$$\mathbf{j}(\mathbf{r}) = 2\pi e T \sum_{n, \mathbf{p}, a} \nu_j \mathbf{v}_F^{(a)} \text{Im} g_a(\mathbf{p}, \mathbf{r}, \omega_n) \quad (\text{S3})$$

where ν_a is the partial density of state, and $g_a = \text{sign}(\omega_n) \sqrt{1 - f_a f_a^+}$.

The Ginzburg-Landau functional, is obtained by expressing the solutions of the Eilenberger equations (S1) as an expansion by powers of the gap functions ampli-

tudes Δ_a and of their gradients:

$$f_a(\mathbf{p}, \mathbf{r}, \omega_n) = \frac{\Delta_a}{\omega_n} - \frac{|\Delta_a|^2 \Delta_a}{2\omega_n^3} - \frac{\hbar(\mathbf{v}_F^{(a)} \mathbf{D})\Delta_a}{2\omega_n^2} + \frac{\hbar^2(\mathbf{v}_F^{(a)} \mathbf{D})(\mathbf{v}_F^{(a)} \mathbf{D})\Delta_a}{4\omega_n^3}. \quad (\text{S4})$$

The summation over the Matsubara frequencies gives

$$2\pi T \sum_{n=0}^{N_d} \omega_n^{-1} = G_0 + \tau, \quad \text{with } \tau = (1 - T/T_c). \quad (\text{S5})$$

Note that, $f_a^+(\mathbf{p}, \mathbf{r}, \omega_n) = f_a^*(-\mathbf{p}, \mathbf{r}, \omega_n)$.

The Ginzburg-Landau equations are determined by the substituting the expansion (S4) into the self-consistency equation (S2). After normalizing the gaps functions by $T_c/\sqrt{\rho}$ (where $\rho = \sum_n \pi T_c^3 \omega_n^{-3} \approx 0.1$), the Ginzburg-Landau equations read as

$$[(G_0 + \tau - \hat{\Lambda}^{-1})\mathbf{\Delta}]_a = -K_{ij}^{(a)} D_i D_j \Delta_a + |\Delta_a|^2 \Delta_a, \quad (\text{S6})$$

where $\mathbf{\Delta} = (\Delta_1, \Delta_2, \Delta_3)^T$, and the anisotropy tensor is $K_{ij}^{(a)} = \hbar^2 \rho \langle v_{F_i}^{(a)} v_{F_j}^{(a)} \rangle / 2T_c^2$. The indices i, j stand for the x, y coordinates, and the average is taken over the a -th Fermi surface. The current reads as

$$\mathbf{J}(\mathbf{r}) = \frac{4e T_c^2}{\hbar \rho} \sum_{a=1}^3 \nu_a \text{Im} \Delta_a^* \hat{K}^{(a)} \mathbf{D} \Delta_a. \quad (\text{S7})$$

The critical temperature is given by the smallest positive eigenvalue of the inverse coupling matrix $\hat{\Lambda}^{-1}$. Namely, if λ_n^{-1} denote the positive eigenvalues of the inverse coupling matrix $\hat{\Lambda}^{-1}$, the critical temperature is determined by the equation $G_0 = \min_n(\lambda_n^{-1})$. Provided that all the eigenvalues are positive, the number of components of the effective field theory coincide with the number of bands. In this case, the Ginzburg-Landau equations for the three-component system read as

$$-K_{ij}^{(a)} D_i D_j \Delta_a + \alpha_{aa} \Delta_a + \alpha_{ab} \Delta_b + \beta_a |\Delta_a|^2 \Delta_a = 0, \quad (\text{S8})$$

where

$$\alpha_{aa} = (\hat{\Lambda}_{ab}^{-1} - G_0 - \tau) \delta_{ab}, \quad (\text{S9a})$$

$$\alpha_{ab} = (1 - \delta_{ab}) \hat{\Lambda}_{ab}^{-1} \quad \text{and} \quad \beta_a = 1. \quad (\text{S9b})$$

While the precise microscopic physics behind the superconductivity in $\text{Ba}_{1-x}\text{K}_x\text{Fe}_2\text{As}_2$ is still unknown, we focus on the scenario of a three-band model with interband dominated repulsive pairing. In this case, the eigenvalues of the inverse coupling matrix are not all positive. This implies, as detailed below, that the three-band theory is described by a two-component order parameter.

B. Two-component Ginzburg-Landau theory for the $s+is$ superconducting state

Our principal interest here, is the time-reversal symmetry breaking $s+is$ state in a three-band superconductor. We consider an interband dominated repulsive pairing, suggested to be relevant for iron-based superconductors [S2]. The corresponding coupling matrix $\hat{\Lambda}$ is parametrized as

$$\hat{\Lambda} = - \begin{pmatrix} 0 & u_{hh} & u_{eh} \\ u_{hh} & 0 & u_{eh} \\ u_{eh} & u_{eh} & 0 \end{pmatrix}. \quad (\text{S10})$$

Thus the fields $\Delta_{1,2}$ correspond to the gap functions at the hole Fermi surfaces while Δ_3 is the gap at the electron pockets sketched in Fig. S1. The coefficients u_{hh} and u_{eh} are respectively the hole-hole and electron-hole interactions. The linear equation that determines the critical temperature $G_0 = \min(G_1, G_2)$ is obtained by neglecting the r.h.s. of (S6). Here G_1 and G_2 are the only two positive eigenvalues of the inverse coupling matrix

$$\hat{\Lambda}^{-1} = \frac{1}{2u_{eh}^2 u_{hh}} \begin{pmatrix} u_{eh}^2 & -u_{eh}^2 & -u_{eh} u_{hh} \\ -u_{eh}^2 & u_{eh}^2 & -u_{eh} u_{hh} \\ -u_{eh} u_{hh} & -u_{eh} u_{hh} & u_{hh}^2 \end{pmatrix}. \quad (\text{S11})$$

They explicitly reads as $G_1 = 1/u_{hh}$ and $G_2 = (u_{hh} + \sqrt{u_{hh}^2 + 8u_{eh}^2})/4u_{eh}^2$. The associated eigenvectors are $\mathbf{\Delta}_1 = (-1, 1, 0)^T$ and $\mathbf{\Delta}_2 = (x, x, 1)^T$, where $x = (u_{hh} - \sqrt{u_{hh}^2 + 8u_{eh}^2})/4u_{eh}$. Since the only fields that can nucleate are those associated with positive eigenvalues, the Ginzburg-Landau theory (S6) has to be reduced to a two-component one. This reduction is obtained by expressing the general order parameter as the linear combination

$$\mathbf{\Delta} = \eta_1 \mathbf{\Delta}_1 + \eta_2 \mathbf{\Delta}_2,$$

$$\text{and } (\Delta_1, \Delta_2, \Delta_3) = (x\eta_2 - \eta_1, x\eta_2 + \eta_1, \eta_2). \quad (\text{S12})$$

Here η_1 and η_2 are the order parameter of the s_{\pm} pairing channels respectively between the two concentric hole surfaces and between the hole and electron surfaces.

The substitution of the linear combination (S12) into the Ginzburg-Landau equations (S6), after projection onto the eigenvectors $\mathbf{\Delta}_{1,2}$, yields the system of two Ginzburg-Landau equations [S1]:

$$a_{11}\eta_1 + b_{1j}|\eta_j|^2\eta_1 + c_{12}\eta_1^*\eta_2^2 = \frac{k_{1j}}{2} \mathbf{D} \mathbf{D} \eta_j, \quad (\text{S13a})$$

$$a_{22}\eta_2 + b_{2j}|\eta_j|^2\eta_2 + c_{12}\eta_2^*\eta_1^2 = \frac{k_{2j}}{2} \mathbf{D} \mathbf{D} \eta_j. \quad (\text{S13b})$$

The parameters on the left hand side of the Ginzburg-Landau equations (S13) are expressed, in terms of the coefficients of the coupling matrix (S10) as

$$a_{jj} = -|\mathbf{\Delta}_j|^2 (G_0 - G_j + \tau), \quad a_{12} = 0 \quad (\text{S14})$$

$$b_{11} = 2, \quad b_{22} = (2x^4 + 1), \quad b_{12} = 4x^2, \quad c_{12} = 2x^2,$$

where $|\Delta_1|^2 = 2$ and $|\Delta_2|^2 = 2x^2 + 1$. The $s + is$ state is symmetric under the C_4 transformations, thus the coefficients satisfy $K_{xx}^{(j)} = K_{yy}^{(j)} = K^{(j)}$. As a results, the coefficients of the gradient terms in (S13) read as

$$k_{11} = 2\xi_0^{-2} [K^{(1)} + K^{(2)}] \quad (\text{S15a})$$

$$k_{22} = 2\xi_0^{-2} [(K^{(1)} + K^{(2)})x^2 + K^{(3)}] \quad (\text{S15b})$$

$$k_{12} = 2\xi_0^{-2} x [K^{(2)} - K^{(1)}]. \quad (\text{S15c})$$

The total superconducting current (S7), is the superposition of the partial currents $\mathbf{J}^{(a)}$ of the different components of the order parameters, as $\mathbf{J} = \sum_a \mathbf{J}^{(a)}$; and the partial currents read as

$$\mathbf{J}^{(a)} = e\text{Im}(\eta_a^* \sum_b [k_{ab} \mathbf{D}\eta_b]). \quad (\text{S16})$$

The two-component free energy functional that corresponds to the Ginzburg-Landau equations (S13), and whose variations with respect to \mathbf{A} give the supercurrent (S16), reads as (in dimensionless units):

$$\mathcal{F} = \frac{\mathbf{B}^2}{2} + \frac{1}{2} \sum_{a,b=1}^2 k_{ab} (\mathbf{D}\eta_a)^* \mathbf{D}\eta_b + V(\boldsymbol{\eta}), \quad (\text{S17a})$$

$$\text{where } V(\boldsymbol{\eta}) = \sum_{a,b=1}^2 a_{ab} \eta_a^* \eta_b + \frac{b_{ab}}{2} |\eta_a|^2 |\eta_b|^2 \quad (\text{S17b})$$

$$+ \frac{c_{12}}{2} (\eta_1^* \eta_2^2 + c.c.). \quad (\text{S17c})$$

Here, the complex fields $\eta_{1,2}$ are the components of the superconducting order parameter. They are electromagnetically coupled by the vector potential \mathbf{A} of the magnetic field $\mathbf{B} = \nabla \times \mathbf{A}$, through the gauge derivative $\mathbf{D} \equiv \nabla + ie\mathbf{A}$. There, the coupling constant e is used to parametrize the London penetration length. Note that for the energy to be positive definite, the coefficients of the kinetic terms should satisfy the relation $\det \hat{k} = k_{11}k_{22} - k_{12}^2 > 0$. Also, for the free energy functional to be bounded from below, the coefficients of the terms that are fourth order in the condensates should satisfy the condition $b_{11}b_{22} - (b_{12} + c_{12})^2 > 0$. Finally, the condition for having a nonzero ground-state density is $\det \hat{a} = a_{11}a_{22} - a_{12}^2 < 0$. These conditions are of course satisfied by the microscopically calculated value (S14) and (S15).

C. Elimination of the mixed-gradients by diagonalization

Within the current basis for the superconducting degrees of freedom, it is quite complicated to deal with the kinetic terms. It is thus worth rewriting the model using a linear combination of the components of the order parameter, that diagonalize the kinetic term:

$$\mathcal{F}_k = \frac{1}{2} \sum_{a,b=1}^2 k_{ab} (\mathbf{D}\eta_a)^* \mathbf{D}\eta_b := \frac{1}{2} (\mathbf{D}\boldsymbol{\eta})^\dagger \hat{k} \mathbf{D}\boldsymbol{\eta}. \quad (\text{S18})$$

Here $\boldsymbol{\eta}^\dagger = (\eta_1^*, \eta_2^*)$, and \hat{k} is the matrix whose elements are k_{ab} . The positive definiteness of the free energy implies that $\det \hat{k} > 0$. So, \hat{k} is a positive definite square matrix whose square root is

$$\mathcal{R} = \frac{\hat{k} + \mathbb{1} \sqrt{\det \hat{k}}}{\sqrt{\text{tr} \hat{k} + 2\sqrt{\det \hat{k}}}}, \text{ where } \hat{k} = \mathcal{R}^\dagger \mathcal{R}. \quad (\text{S19})$$

This determines a natural linear combination of the superconducting degrees of freedom, where the kinetic term (S18) is diagonal:

$$\mathcal{F}_k = \frac{1}{2} (\mathbf{D}\Psi)^\dagger \mathbf{D}\Psi, \text{ where } \Psi = \mathcal{R}\boldsymbol{\eta}, \quad (\text{S20})$$

and $\Psi^\dagger = (\psi_1^*, \psi_2^*)$. The original superconducting degrees of freedom $\boldsymbol{\eta}$ are restored via the reverse transformation $\boldsymbol{\eta} = \mathcal{R}^{-1}\Psi$, where

$$\mathcal{R}^{-1} = \frac{\sqrt{\text{tr} \hat{k} + 2\sqrt{\det \hat{k}}}}{\det(\hat{k} + \mathbb{1} \sqrt{\det \hat{k}})} [(\text{tr} \hat{k} + \sqrt{\det \hat{k}}) \mathbb{1} - \hat{k}]. \quad (\text{S21})$$

Using the relations (S19) and (S21) to parametrize the superconducting degrees of freedom with Ψ instead of $\boldsymbol{\eta}$, greatly simplifies the kinetic term (S20). Thus, the potential term in the free energy (S17) has to be rewritten in terms Ψ . In all generality, the potential energy reads as

$$\mathcal{F}_p := V(\boldsymbol{\eta}) = a_{ij} \eta_i^* \eta_j + \frac{b_{ijkl}}{2} \eta_i^* \eta_j^* \eta_k \eta_l, \quad (\text{S22})$$

with the summation over the repeated indices. Note that for the energy to be a real quantity, the tensor coefficients a_{ij} , and b_{ijkl} should obey some symmetry relations:

$$a_{ij} = a_{ji} \quad (\text{S23a})$$

$$b_{ijkl} = b_{jikl} = b_{ijlk} = b_{klij}. \quad (\text{S23b})$$

Similarly, in terms of Ψ the potential energy reads as

$$\mathcal{F}_p := V(\Psi) = \alpha_{ij} \psi_i^* \psi_j + \frac{\beta_{ijkl}}{2} \psi_i^* \psi_j^* \psi_k \psi_l, \quad (\text{S24})$$

where the tensor coefficients α_{ij} and β_{ijkl} obey the same symmetry relations (S23) as a_{ij} , and b_{ijkl} . They are obtained via the transformation $\boldsymbol{\eta} = \mathcal{R}^{-1}\Psi$, and the relations are

$$\alpha_{ij} = a_{ab} \mathcal{R}_{ai}^{-1} \mathcal{R}_{bj}^{-1} \quad (\text{S25a})$$

$$\beta_{ijkl} = b_{abcd} \mathcal{R}_{ai}^{-1} \mathcal{R}_{bj}^{-1} \mathcal{R}_{ck}^{-1} \mathcal{R}_{dl}^{-1}. \quad (\text{S25b})$$

A simple, yet lengthy algebraic manipulations thus yield the free energy in terms of the superconducting degrees of freedom Ψ

$$\mathcal{F} = \frac{\mathbf{B}^2}{2} + \frac{1}{2}(\mathbf{D}\Psi)^\dagger \mathbf{D}\Psi + V(\Psi), \quad \text{where } \mathbf{B} = \nabla \times \mathbf{A}, \quad \mathbf{D} \equiv \nabla + ie\mathbf{A}, \quad (\text{S26a})$$

$$\text{and } V(\Psi) = \sum_{i,j=1}^2 \alpha_{ij} \psi_i^* \psi_j + \frac{\beta_{ij}}{2} |\psi_i|^2 |\psi_j|^2 + (\gamma_{11} |\psi_1|^2 + \gamma_{22} |\psi_2|^2) (\psi_1^* \psi_2 + c.c.) + \frac{\gamma_{12}}{2} (\psi_1^* \psi_2^2 + c.c.), \quad (\text{S26b})$$

and $\beta_{ij} := \beta_{ijkl} \delta_{ki} \delta_{jl}$, $\gamma_{ik} = \beta_{ijkl} \delta_{j1} \delta_{l2}$. Moreover, all the coefficients are symmetric, for example $\beta_{21} = \beta_{12}$. Using the relations (S25), and collecting the various terms yields the relation for the coefficients of the bilinear terms

$$\alpha_{11} = a_{11}(\mathcal{R}_{11}^{-1})^2 + a_{22}(\mathcal{R}_{21}^{-1})^2 + 2a_{12}\mathcal{R}_{11}^{-1}\mathcal{R}_{21}^{-1} \quad (\text{S27a})$$

$$\alpha_{22} = a_{11}(\mathcal{R}_{12}^{-1})^2 + a_{22}(\mathcal{R}_{22}^{-1})^2 + 2a_{12}\mathcal{R}_{12}^{-1}\mathcal{R}_{22}^{-1} \quad (\text{S27b})$$

$$\alpha_{12} = a_{11}\mathcal{R}_{11}^{-1}\mathcal{R}_{12}^{-1} + a_{22}\mathcal{R}_{21}^{-1}\mathcal{R}_{22}^{-1} + a_{12}(\mathcal{R}_{11}^{-1}\mathcal{R}_{22}^{-1} + \mathcal{R}_{12}^{-1}\mathcal{R}_{21}^{-1}). \quad (\text{S27c})$$

Similarly, the coefficients for the fourth order terms are

$$\beta_{11} = \frac{b_{11}}{2}(\mathcal{R}_{11}^{-1})^4 + \frac{b_{22}}{2}(\mathcal{R}_{21}^{-1})^4 + (b_{12} + c_{12})(\mathcal{R}_{11}^{-1})^2(\mathcal{R}_{21}^{-1})^2 + 2\mathcal{R}_{11}^{-1}\mathcal{R}_{21}^{-1}(c_{11}(\mathcal{R}_{11}^{-1})^2 + c_{22}(\mathcal{R}_{21}^{-1})^2) \quad (\text{S28a})$$

$$\beta_{22} = \frac{b_{11}}{2}(\mathcal{R}_{12}^{-1})^4 + \frac{b_{22}}{2}(\mathcal{R}_{22}^{-1})^4 + (b_{12} + c_{12})(\mathcal{R}_{12}^{-1})^2(\mathcal{R}_{22}^{-1})^2 + 2\mathcal{R}_{12}^{-1}\mathcal{R}_{22}^{-1}(c_{11}(\mathcal{R}_{12}^{-1})^2 + c_{22}(\mathcal{R}_{22}^{-1})^2) \quad (\text{S28b})$$

$$\beta_{12} = 2b_{11}(\mathcal{R}_{11}^{-1})^2(\mathcal{R}_{12}^{-1})^2 + 2b_{22}(\mathcal{R}_{21}^{-1})^2(\mathcal{R}_{22}^{-1})^2 + b_{12}(\mathcal{R}_{11}^{-1}\mathcal{R}_{22}^{-1} + \mathcal{R}_{12}^{-1}\mathcal{R}_{21}^{-1})^2 + 4c_{12}\mathcal{R}_{11}^{-1}\mathcal{R}_{12}^{-1}\mathcal{R}_{21}^{-1}\mathcal{R}_{22}^{-1} + 4(c_{11}\mathcal{R}_{11}^{-1}\mathcal{R}_{12}^{-1} + c_{22}\mathcal{R}_{21}^{-1}\mathcal{R}_{22}^{-1})(\mathcal{R}_{11}^{-1}\mathcal{R}_{22}^{-1} + \mathcal{R}_{12}^{-1}\mathcal{R}_{21}^{-1}), \quad (\text{S28c})$$

and

$$\gamma_{11} = b_{11}(\mathcal{R}_{11}^{-1})^3\mathcal{R}_{21}^{-1} + b_{22}(\mathcal{R}_{12}^{-1})^3\mathcal{R}_{22}^{-1} + (b_{12} + c_{12})\mathcal{R}_{11}^{-1}\mathcal{R}_{21}^{-1}(\mathcal{R}_{11}^{-1}\mathcal{R}_{22}^{-1} + \mathcal{R}_{12}^{-1}\mathcal{R}_{21}^{-1}) + c_{11}(\mathcal{R}_{11}^{-1})^2(\mathcal{R}_{11}^{-1}\mathcal{R}_{22}^{-1} + 3\mathcal{R}_{12}^{-1}\mathcal{R}_{21}^{-1}) + c_{22}(\mathcal{R}_{12}^{-1})^2(3\mathcal{R}_{11}^{-1}\mathcal{R}_{22}^{-1} + \mathcal{R}_{12}^{-1}\mathcal{R}_{21}^{-1}) \quad (\text{S29a})$$

$$\gamma_{22} = b_{11}(\mathcal{R}_{21}^{-1})^3\mathcal{R}_{11}^{-1} + b_{22}(\mathcal{R}_{22}^{-1})^3\mathcal{R}_{12}^{-1} + (b_{12} + c_{12})\mathcal{R}_{22}^{-1}\mathcal{R}_{12}^{-1}(\mathcal{R}_{11}^{-1}\mathcal{R}_{22}^{-1} + \mathcal{R}_{12}^{-1}\mathcal{R}_{21}^{-1}) + c_{11}(\mathcal{R}_{12}^{-1})^2(3\mathcal{R}_{11}^{-1}\mathcal{R}_{22}^{-1} + \mathcal{R}_{12}^{-1}\mathcal{R}_{21}^{-1}) + c_{22}(\mathcal{R}_{22}^{-1})^2(\mathcal{R}_{11}^{-1}\mathcal{R}_{22}^{-1} + 3\mathcal{R}_{12}^{-1}\mathcal{R}_{21}^{-1}) \quad (\text{S29b})$$

$$\gamma_{12} = \frac{b_{11}}{2}(\mathcal{R}_{11}^{-1})^2(\mathcal{R}_{12}^{-1})^2 + \frac{b_{22}}{2}(\mathcal{R}_{21}^{-1})^2(\mathcal{R}_{22}^{-1})^2 + b_{12}\mathcal{R}_{11}^{-1}\mathcal{R}_{12}^{-1}\mathcal{R}_{21}^{-1}\mathcal{R}_{22}^{-1} + \frac{c_{12}}{2}((\mathcal{R}_{11}^{-1}\mathcal{R}_{22}^{-1})^2 + (\mathcal{R}_{12}^{-1}\mathcal{R}_{21}^{-1})^2) + (c_{11}\mathcal{R}_{11}^{-1}\mathcal{R}_{12}^{-1} + c_{22}\mathcal{R}_{21}^{-1}\mathcal{R}_{22}^{-1})(\mathcal{R}_{11}^{-1}\mathcal{R}_{22}^{-1} + \mathcal{R}_{12}^{-1}\mathcal{R}_{21}^{-1}). \quad (\text{S29c})$$

Note that the elimination of the mixed gradient terms via the decomposition of the matrix \hat{k} in terms of the square root matrix \mathcal{R} is not unique. Indeed, there exist different possibilities, see for example [S1, S32].

D. Separation of charged and neutral modes

The total Meissner current \mathbf{J} is defined by the variation of the free energy (S26) with respect to the vector potential:

$$\mathbf{J} := \frac{\delta \mathcal{F}}{\delta \mathbf{A}} = e^2 \Psi^\dagger \Psi \mathbf{A} + e \text{Im}(\Psi^\dagger \nabla \Psi). \quad (\text{S30})$$

It follows that the gauge field can be explicitly eliminated by expressing \mathbf{A} in terms of the condensate Ψ , and the Meissner current:

$$e\mathbf{A} = \frac{1}{e\rho^2} \left(\mathbf{J} - e \text{Im}(\Psi^\dagger \nabla \Psi) \right), \quad \text{where } \rho^2 = \Psi^\dagger \Psi. \quad (\text{S31})$$

Indeed, the kinetic term can be written as

$$|\mathbf{D}\Psi|^2 = \frac{\mathbf{J}^2}{e^2 \rho^2} + \nabla \Psi^\dagger \cdot \nabla \Psi + \frac{(\Psi^\dagger \nabla \Psi - \nabla \Psi^\dagger \Psi)^2}{4\rho^2}, \quad (\text{S32})$$

and that the magnetic field

$$B_k = \epsilon_{kij} \left\{ \nabla_i \left(\frac{J_j}{e^2 \rho^2} \right) + \frac{i}{e\rho^4} Z_{ij} \right\} \quad (\text{S33a})$$

$$\text{where } Z_{ij} = \rho^2 \nabla_i \Psi^\dagger \nabla_j \Psi + (\Psi^\dagger \nabla_i \Psi)(\nabla_j \Psi^\dagger \Psi). \quad (\text{S33b})$$

Hence, the magnetic field features a contribution from the Meissner current \mathbf{J} , together with a contribution from the interband counterflow Z_{ij} . Note that since $Z_{ij}^* = Z_{ji}$, the magnetic field can be written as

$$B_k = \epsilon_{kij} \left\{ \nabla_i \left(\frac{J_j}{e^2 \rho^2} \right) - \frac{\text{Im} Z_{ij}}{e\rho^4} \right\}. \quad (\text{S34})$$

It follows that the free energy (S26) can be rewritten as

$$\mathcal{F} = \frac{1}{2} \left[\epsilon_{kij} \left\{ \nabla_i \left(\frac{J_j}{e^2 \varrho^2} \right) + \frac{i}{e \varrho^4} Z_{ij} \right\} \right]^2 + \frac{\mathbf{J}^2}{2e^2 \varrho^2} + \nabla \Psi^\dagger \cdot \nabla \Psi + \frac{1}{4\varrho^2} (\Psi^\dagger \nabla \Psi - \nabla \Psi^\dagger \Psi)^2 + V(\Psi), \quad (\text{S35})$$

where Z_{ij} is defined in (S33b).

E. Mapping to the effective model

Two-component Ginzburg-Landau models can often be mapped onto a version of the nonlinear O(3) σ -model [S1, S4–S6]. In those mappings the O(3) symmetry is explicitly broken by the potential terms, consistently with the symmetry of the superconducting state. The mapping couples the massive U(1) vector field (the current \mathbf{J}) to a compact O(3) unit vector (the pseudo-spin \mathbf{n}) and a real scalar (the density ϱ). The pseudo-spin unit is defined by projecting the superconducting degrees of freedom onto the spin-1/2 Pauli matrices σ . For derivation of this mapping for different two-component Ginzburg-Landau models, see *e.g.* [S1, S6].

Here, we use an alternative mapping to a model that couples the massive U(1) vector field (the current \mathbf{J}) to the fermion quadrupling order parameter in the form of a 3-vector \mathbf{m} . The fermion quadrupling field is defined as the projection of the superconducting degrees of freedom Ψ onto the spin-1/2 Pauli matrices σ :

$$\mathbf{m} \equiv (m_x, m_y, m_z) = \Psi^\dagger \sigma \Psi. \quad (\text{S36})$$

Unlike the pseudo-spin \mathbf{n} , which a unit vector, the norm of \mathbf{m} is not fixed. Thus \mathbf{n} and \mathbf{m} are related to each other according to $\mathbf{m} = \varrho^2 \mathbf{n}$, and we sometime refer to \mathbf{m} as a soft modulus vector field. The projection (S36) determines the following relations

$$\begin{aligned} \partial_i \mathbf{m} \cdot \partial_j \mathbf{m} &= 2\rho^2 (\partial_i \Psi^\dagger \partial_j \Psi + \partial_j \Psi^\dagger \partial_i \Psi) \\ &+ (\Psi^\dagger \partial_i \Psi - \partial_i \Psi^\dagger \Psi) (\Psi^\dagger \partial_j \Psi - \partial_j \Psi^\dagger \Psi), \end{aligned} \quad (\text{S37})$$

where, for the product of Pauli matrices, we used the Fierz identity

$$\sigma_{ab}^\alpha \sigma_{cd}^\alpha = 2\delta_{ad}\delta_{bc} - \delta_{ab}\delta_{cd}, \quad (\text{S38})$$

where δ_{ab} is the Kronecker symbol. It follows that

$$(\nabla \mathbf{m})^2 = 4\rho^2 \nabla \Psi^\dagger \cdot \nabla \Psi + (\Psi^\dagger \nabla \Psi - \nabla \Psi^\dagger \Psi)^2. \quad (\text{S39})$$

The kinetic term (S32) can thus be written as

$$|D\Psi|^2 = \frac{\mathbf{J}^2}{e^2 \varrho^2} + \frac{1}{4\varrho^2} (\nabla \mathbf{m})^2. \quad (\text{S40})$$

Similarly, the projection (S36) determines the relation

$$\begin{aligned} \mathbf{m} \cdot \partial_i \mathbf{m} \times \partial_j \mathbf{m} &= -2i\varrho^4 (\partial_i \Psi^\dagger \partial_j \Psi - \partial_j \Psi^\dagger \partial_i \Psi) \\ &- 2i\varrho^2 [(\Psi^\dagger \partial_i \Psi)(\partial_j \Psi^\dagger \Psi) - (\partial_i \Psi^\dagger \Psi)(\Psi^\dagger \partial_j \Psi)], \end{aligned} \quad (\text{S41})$$

where, for the triple product of Pauli matrices, we used the identity

$$\epsilon_{\alpha\beta\gamma} \sigma_{ab}^\alpha \sigma_{cd}^\beta \sigma_{ef}^\gamma = 2i(\delta_{af}\delta_{bc}\delta_{de} - \delta_{ad}\delta_{cf}\delta_{be}). \quad (\text{S42})$$

There δ_{ab} is the Kronecker symbol, and $\epsilon_{\alpha\beta\gamma}$ is the rank-3 Levi-Civita symbol. It follows that

$$\begin{aligned} \epsilon_{ijk} \mathbf{m} \cdot \partial_i \mathbf{m} \times \partial_j \mathbf{m} &= \\ &- 4i\varrho^2 \epsilon_{ijk} \left\{ \varrho^2 \partial_i \Psi^\dagger \partial_j \Psi + (\Psi^\dagger \partial_i \Psi)(\partial_j \Psi^\dagger \Psi) \right\}. \end{aligned} \quad (\text{S43})$$

Hence, the magnetic field reads as

$$\mathbf{B} = \nabla \times \left(\frac{\mathbf{J}}{e^2 \varrho^2} \right) - \frac{\epsilon_{\alpha\beta\gamma}}{4e\varrho^6} m_\alpha \nabla m_\beta \times \nabla m_\gamma. \quad (\text{S44})$$

As a result,

$$\begin{aligned} \mathcal{F} &= \frac{1}{2} \left[\epsilon_{kij} \left\{ \nabla_i \left(\frac{J_j}{e^2 \varrho^2} \right) - \frac{1}{4e\varrho^6} \mathbf{m} \cdot \partial_i \mathbf{m} \times \partial_j \mathbf{m} \right\} \right]^2 \\ &+ \frac{\mathbf{J}^2}{2e^2 \varrho^2} + \frac{1}{8\varrho^2} (\nabla \mathbf{m})^2 + V(\mathbf{m}), \end{aligned} \quad (\text{S45})$$

where the density is $\varrho^2 \equiv \|\mathbf{m}\| = \sqrt{\mathbf{m} \cdot \mathbf{m}}$.

The effective model of the fermion quadrupling resistive state is deduced by removing the superconducting degrees of freedom from (S45), since their prefactors are renormalized to zero. Namely, in that resistive state the Meissner current vanishes ($\mathbf{J} = 0$), while the currents associated with the gradients of the fermion quadrupling order parameter \mathbf{m} do not. Assuming that the critical temperatures of \mathbb{Z}_2 and U(1) transitions are well separated, and assuming a mean-field approximation for the fields that are fourth-order in fermions the free energy of the fermion quadrupling state reads as

$$\mathcal{F} = \frac{(\mathbf{m} \cdot \partial_i \mathbf{m} \times \partial_j \mathbf{m})^2}{16e^2 \|\mathbf{m}\|^6} + \frac{(\nabla \mathbf{m})^2}{8\|\mathbf{m}\|} + V(\mathbf{m}). \quad (\text{S46})$$

Similarly, the magnetic field in the fermion quadrupling resistive state becomes

$$\mathbf{B} = -\frac{\epsilon_{\alpha\beta\gamma} m_\alpha \nabla m_\beta \times \nabla m_\gamma}{4e\|\mathbf{m}\|^3}. \quad (\text{S47})$$

Equivalently, component-wise, the magnetic field is

$$B_k = -\frac{\epsilon_{kij} \mathbf{m} \cdot \nabla_i \mathbf{m} \times \nabla_j \mathbf{m}}{4e\|\mathbf{m}\|^3}. \quad (\text{S48})$$

Finally, the potential term reads as

$$V(\mathbf{m}) = \sum_{a=0,x,y,z} \left(\alpha_a^{\mathbf{m}} + \sum_{b=0,x,y,z} \frac{\beta_{ab}^{\mathbf{m}}}{2} m_b \right) m_a, \quad (\text{S49})$$

where the component $m_0 := \|\mathbf{m}\|$, and the coefficients depend on the coefficients (S27), (S28) and (S29) of the

diagonalized free-energy (S26). All the coefficients involving a y index vanish: $\alpha_y^{\mathbf{m}} = \beta_{ay}^{\mathbf{m}} = \beta_{ya}^{\mathbf{m}} = 0$. The non-zero coefficients $\alpha_a^{\mathbf{m}}$ of the linear term in m_a are

$$\alpha_0^{\mathbf{m}} = \frac{\alpha_{11} + \alpha_{22}}{2}, \quad \alpha_x^{\mathbf{m}} = \alpha_{12}, \quad \alpha_z^{\mathbf{m}} = \frac{\alpha_{11} - \alpha_{22}}{2}. \quad (\text{S50})$$

Next, the non-zero coefficients $\beta_{ab}^{\mathbf{m}}$ of the bilinear term in m_a are

$$\beta_{00}^{\mathbf{m}} = \frac{\beta_{11} + \beta_{22} + 2(\beta_{12} - \gamma_{12})}{4}, \quad (\text{S51a})$$

$$\beta_{0x}^{\mathbf{m}} = \beta_{x0}^{\mathbf{m}} = \frac{\gamma_{11} + \gamma_{22}}{2}, \quad (\text{S51b})$$

$$\beta_{0z}^{\mathbf{m}} = \beta_{z0}^{\mathbf{m}} = \frac{\beta_{11} - \beta_{22}}{2}, \quad (\text{S51c})$$

and

$$\beta_{xx}^{\mathbf{m}} = \gamma_{12}, \quad (\text{S52a})$$

$$\beta_{xz}^{\mathbf{m}} = \beta_{zx}^{\mathbf{m}} = \frac{\gamma_{11} - \gamma_{22}}{2}, \quad (\text{S52b})$$

$$\beta_{zz}^{\mathbf{m}} = \frac{\beta_{11} + \beta_{22} - 2(\beta_{12} - \gamma_{12})}{4}. \quad (\text{S52c})$$

Topological properties in two-dimensions

The soft modulus vector field \mathbf{m} (S36) can be associated with non-trivial topological properties, by considering the properties of the corresponding unit vector field $\mathbf{n} := \mathbf{m}/\|\mathbf{m}\|$. Indeed, the unit vector \mathbf{n} is a map from the one-point compactification of the plane ($\mathbb{R}^2 \cup \{\infty\} \cong \mathbb{S}^2$) onto the two-sphere target space spanned by \mathbf{n} . That is $\mathbf{n} : \mathbb{S}^2 \mapsto \mathbb{S}_n^2$, which is classified by the homotopy class $\pi_2(\mathbb{S}_n^2) \in \mathbb{Z}$, thus defining the topological invariant, *i.e.* the degree of the map, as

$$\mathcal{Q}(\mathbf{n}) = \frac{1}{4\pi} \int_{\mathbb{R}^2} \mathbf{n} \cdot \partial_x \mathbf{n} \times \partial_y \mathbf{n} \, dx dy. \quad (\text{S53})$$

Note that \mathbf{n} is ill-defined when $\|\mathbf{m}\| = 0$. On the other hand, whenever $\|\mathbf{m}\| \neq 0$, the corresponding configuration have an integer topological charge $\mathcal{Q}(\mathbf{n}) \in \mathbb{Z}$. In a way, $\mathcal{Q}(\mathbf{n})$ counts the number of times the pseudo-spin texture of \mathbf{n} wraps the target two-sphere. The topological invariant (S53), the index of the map \mathbf{n} , can be expressed directly in terms of the soft modulus vector field \mathbf{m} . This is easily done by replacing \mathbf{n} with its actual definition $\mathbf{n} := \mathbf{m}/\|\mathbf{m}\|$. The topological invariant thus reads as

$$\mathcal{Q}(\mathbf{m}) = \frac{1}{4\pi} \int_{\mathbb{R}^2} \frac{\mathbf{m} \cdot \partial_x \mathbf{m} \times \partial_y \mathbf{m}}{\|\mathbf{m}\|^3} \, dx dy. \quad (\text{S54})$$

Here again, the integrand is obviously ill-defined when $\|\mathbf{m}\| = 0$. Whenever $\|\mathbf{m}\| \neq 0$, the corresponding configuration have an integer topological charge $\mathcal{Q}(\mathbf{m}) \in \mathbb{Z}$. The quantization of $\mathcal{Q}(\mathbf{m})$ implies that the magnetic flux is quantized as well according to $\int \mathbf{B}_z = \Phi_0 \mathcal{Q}$, where $\Phi_0 = -2\pi/e$ is the flux quantum.

It should be emphasized that unlike the flux quantization condition for the superconducting states, which is related to the U(1) topological invariant, the condition (S54) is also valid in the non-superconducting phase. Indeed, the quantization in the superconducting state is given by the U(1) topological invariant, which is related to the total phase winding at spatial infinity (the usual winding number). In the fermion quadrupling resistive state, the total phase of Ψ is disordered and the U(1) invariant does not exist. On the other, since it is associated only with the relative phases, $\mathcal{Q}(\mathbf{m})$ is the quantity that defines the flux quantization.

It is worth emphasizing that the topological charge (S53) is an integer, when integrated over the infinite plane \mathbb{R}^2 , or at least an large enough domain $\Omega \subset \mathbb{R}^2$.

F. Parameter sets

The essential features can be qualitatively summarized as follows: First, all the coefficients involving a y index vanish: $\alpha_y^{\mathbf{m}} = \beta_{ay}^{\mathbf{m}} = \beta_{ya}^{\mathbf{m}} = 0$. Moreover, the criterion for the condensation is $\alpha_0^{\mathbf{m}^2} > \alpha_x^{\mathbf{m}^2} + \alpha_z^{\mathbf{m}^2}$, and also $\beta_{00}^{\mathbf{m}}, \beta_{zz}^{\mathbf{m}} > 0$. The effect of the time-reversal symmetry operation for the soft modulus vector is a reflection of \mathbf{m} on the xz -plane of the target space:

$$\mathcal{T}(\Psi) = \Psi^* \Leftrightarrow \mathcal{T}(\mathbf{m}) = (m_x, -m_y, m_z). \quad (\text{S55})$$

A typical value of the parameter set, when obtained from the microscopic model, is given in the Table I.

G. Modulation of the parameters

Inhomogeneities in a sample typically result in spatially varying parameters of the Ginzburg-Landau model. In the system with broken time-reversal symmetry this can result in gradients of both densities and relative phases. This can in principle produce spontaneous magnetic fields. As emphasized in the main body, the material has slight inhomogeneity in the doping level, and this results in relatively small local modulation of the superconducting critical temperature. This can be accounted for by implementing spatial modulation of the prefactors of the quadratic terms of the Ginzburg-Landau theory. For example, the parameters of the quadratic term of the original Ginzburg-Landau theory (S17) formally depend on the temperature, $a_{ii} \equiv a_{ii}(\tau) = a_{ii}^0[\tau - 1]$. Hence, it may be possible to model the effect of temperature inhomogeneities by requiring a spatial dependence of the parameters $a_{ii} \equiv a_{ii}(\tau, \mathbf{x}) = a_{ii}^0[\tau(\mathbf{x}) - 1]$. Different areas of an inhomogeneous sample indeed can have different local critical temperatures. Such a local modification of the parameter was demonstrated to be responsible for the existence of spontaneous magnetic fields, in different models with time-reversal symmetry breaking states. These include the responses to linear thermal gradients

Parameters of the effective model	α_0^m ($\times 10^{-1}$)	α_x^m ($\times 10^{-2}$)	α_z^m ($\times 10^{-2}$)	β_{00}^m ($\times 10^{-1}$)	β_{0x}^m ($\times 10^{-2}$)	β_{0z}^m ($\times 10^{-2}$)	β_{xx}^m ($\times 10^{-1}$)	β_{xz}^m ($\times 10^{-2}$)	β_{zz}^m ($\times 10^{-1}$)
	-8.2605	8.0923	-6.3919	4.5431	-6.5085	1.4987	2.1940	-0.0875	2.3491

Table I. Coefficients of the Ginzburg-Landau free energy functional that correspond to the various numerical simulations reported in the main body of the text. Starting from the microscopic model (S10), the parameters of the coupling matrix are $u_{ch} = 0.45$ and $u_{hh} = 0.5$, and the coefficients of the gradient term are $K^{(1)} = 0.5$, $K^{(2)} = 0.35$, $K^{(3)} = 0.45$ and the temperature parameter is $T/T_c = 0.25$. Next, the coefficients of the diagonalized Ginzburg-Landau model (S26) are evaluated using the formulas (S27), (S28) and (S29). Finally the coefficients of the soft modulus effective model are obtained with the formulas (S50), (S51), and (S52).

[S7, S8], hotspot created by a laser pulse [S9] but also the effect of impurities [S10, S11], and other inhomogeneous arrays [S3, S12].

At the level of the effective model, implementing smoothly spatially varying amplitudes of the individual components, can be modelled by small spatial variations of the coupling constants α_0^m and α_z^m accordingly, given the relations (S27) and (S50). In the main body, we considered random modulations in the form of $\tau(\mathbf{x}) = \tau_0[1 + \delta\tau \text{ran}(\mathbf{x})]$ where $\text{ran}(\mathbf{x})$ is a smooth random surface. Here τ_0 is the nominal reduced temperature, $\delta\tau$ is the amplitude of the thermal variation. The idea to construct a random, smoothly varying quantity is to represent it as a Fourier series with random coefficients:

$$f(\mathbf{x}) = -c_0 + \sum_{i=1}^{N_x} \sum_{j=1}^{N_y} c_{ij} \cos 2\pi \left(\frac{ix}{L_x} + \frac{jy}{L_y} \right) + s_{ij} \sin 2\pi \left(\frac{ix}{L_x} + \frac{jy}{L_y} \right), \quad (\text{S56})$$

were L_x and L_y are the dimensions of the box that bounds the numerical domain. N_x and N_y are cut-off in the Fourier expansion, and the coefficients c_{ij} and s_{ij} are random numbers $\in [-0.5 : 0.5]$.

II. NUMERICAL METHODS

In the numerical investigations in the main body of the paper, we use Finite-Element Methods (FEM) (see e.g. [S13, S14]) to handle the spatial discretization of the problem. In practice we use the finite-element framework provided by the FreeFEM library [S15]. Within this finite-element framework, the minimization of the free energy is addressed using a non-linear conjugate gradient algorithm [S16–S19].

A. Finite-element formulation

We consider the domain Ω which a bounded open subset of \mathbb{R}^2 and denote $\partial\Omega$ its boundary. $H(\Omega)$ stands for the Hilbert space, such that a function belonging to $H(\Omega)$, and its weak derivatives have a finite L^2 -norm.

Furthermore. The Hilbert spaces of real-valued functions is equipped with the inner product $\langle \cdot, \cdot \rangle$, defined as:

$$\langle u, v \rangle = \int_{\Omega} uv, \text{ for } u, v \in H(\Omega). \quad (\text{S57})$$

The spatial domain Ω is discretized as a mesh of triangles using for the Delaunay-Voronoi algorithm, and the regular partition \mathcal{T}_h of Ω refers to the family of the triangles that compose the mesh. Given a spatial discretization, the functions are approximated to belong to a *finite-element space* whose properties correspond to the details of the Hilbert spaces to which the functions belong. We define $P_h^{(2)}$ as the 2-nd order Lagrange finite-element subspace of $H(\Omega)$. Now, the physical degrees of freedom can be discretized in their finite element subspaces. And we define the finite-element description of the degrees of freedom as $m_i \mapsto m_i^{(h)} \in \mathcal{P}_h^{(2)}$. This describes a linear vector space of finite dimension, for which a basis can be found. The canonical basis consists of the shape functions $\phi_k(\mathbf{x})$, and thus

$$V_h(\mathcal{T}_h, P^{(2)}) = \left\{ w(\mathbf{x}) = \sum_{k=1}^M w_k \phi_k(\mathbf{x}), \phi_k(\mathbf{x}) \in P_h^{(2)} \right\}. \quad (\text{S58})$$

Here M is the dimension of V_h (the number of vertices), the w_k are called the degrees of freedom of w and M the number of the degrees of freedom. To summarize, a given function is approximated as its decomposition: $w(\mathbf{x}) = \sum_{k=1}^M w_k \phi_k(\mathbf{x})$, on a given basis of shape functions $\phi_k(\mathbf{x})$ of the polynomial functions $P^{(2)}$ for the triangle T_{i_k} . The finite element space $V_h(\mathcal{T}_h, P^{(2)})$ hence denotes the space of continuous, piecewise quadratic functions of x , y on each triangle of \mathcal{T}_h .

B. Initial guess: Skyrmions and domain-walls

The skyrmions and the domain-walls are field configurations for the two-dimensional system. More precisely, either for the true two-dimensional system, or for a three-dimensional system with a translational invariance along the third direction z . The initial guess is defined, such that the ground state would be $m_z = \pm 1$. The configuration is then rotated using the rotation matrices R_i and scaled to match the actual ground state $\hat{\mathbf{m}}$:

$$\mathbf{m} = r_0 R_z(-\varphi_0) R_y(-\theta_0) \mathcal{S}^{(sk)} \mathbf{n}^{(dw)}. \quad (\text{S59})$$

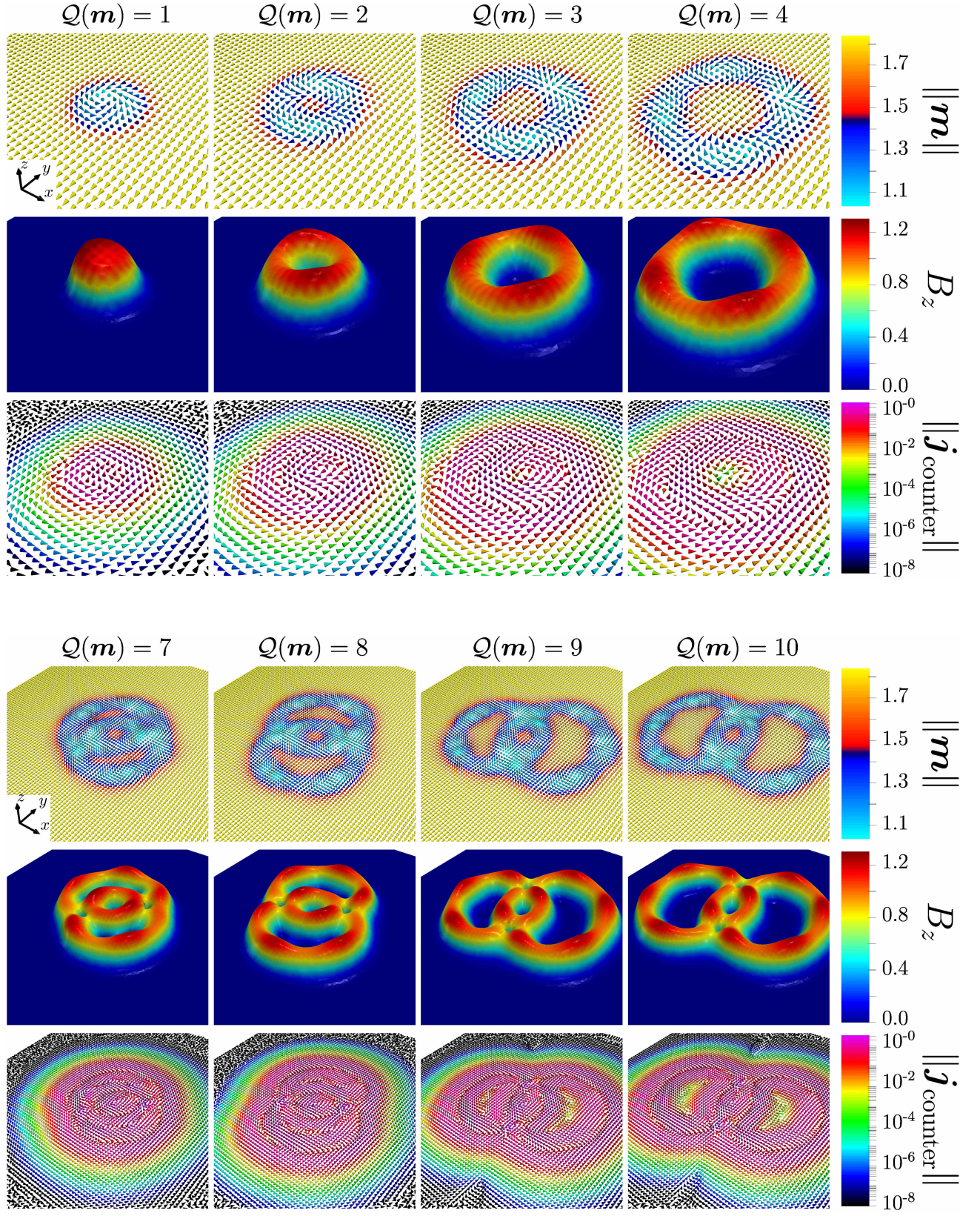


Figure S2. Skyrmion solutions in a time-reversal symmetry broken state, for increasing values of the topological charge $Q(\mathbf{m})$. On each block, the panels on the top row display the texture of the four-fermion order parameter \mathbf{m} . The panels on the middle row show the associated magnetic field \mathbf{B} (S47), and the bottom row display the corresponding charge transferring counter-currents $\mathbf{j}_{\text{counter}}$ according to the Ampère's law. The parameters are the same as in the main body. Note that as can be seen from the densities of arrows, the configurations for $Q(\mathbf{m})=7-10$ are zoomed out, as compared to those for $Q(\mathbf{m})=1-4$.

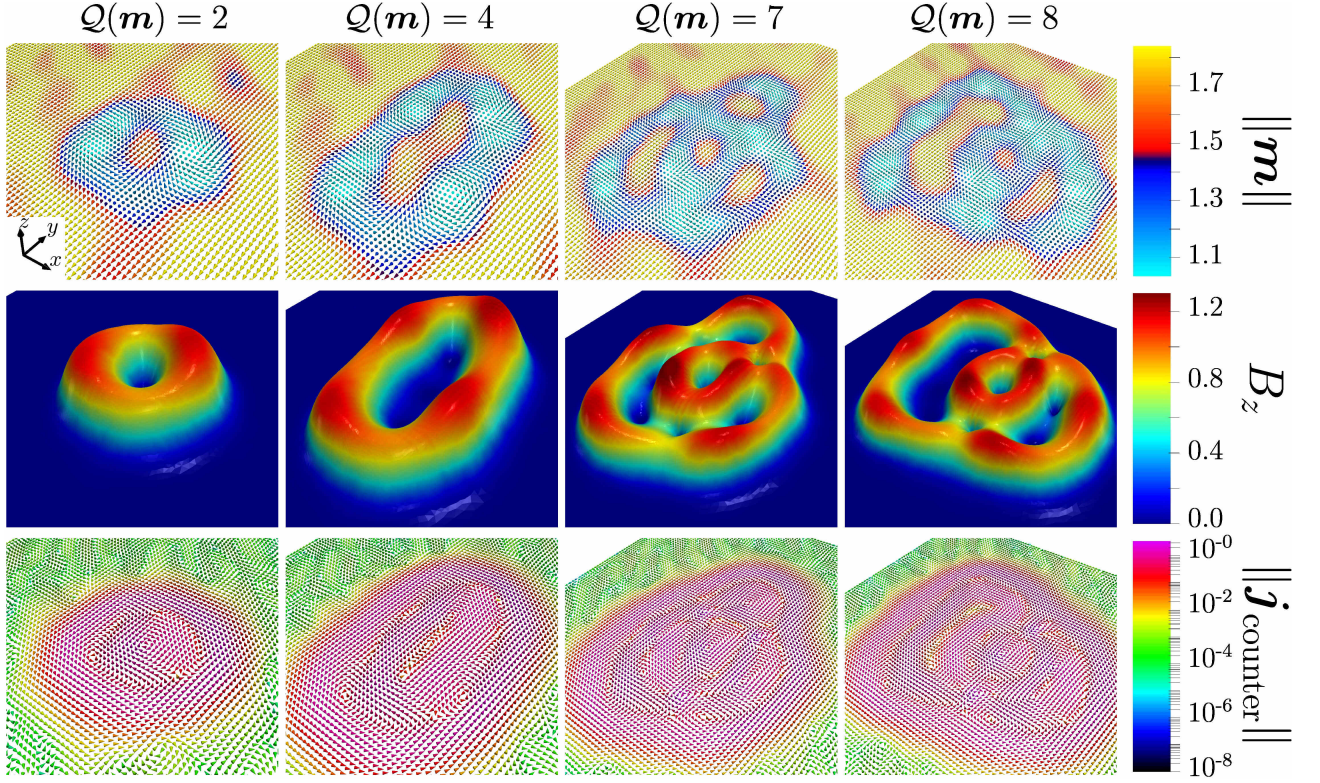


Figure S3. Skymion solutions in the presence of inhomogeneities. On each block, the panels on the top row display the texture of the four-fermion order parameter \mathbf{m} . The panels on the middle row show the associated magnetic field \mathbf{B} (S47), and the bottom row display the corresponding charge transferring counter-currents $\mathbf{j}_{\text{counter}}$ according to the Ampère's law. The parameters are the same as in the main body. Note that as can be seen from the densities of arrows, the configurations for $Q(\mathbf{m})=7,8$ are zoomed out, as compared to those for $Q(\mathbf{m})=2,4$.

Here $r_0 = \|\hat{m}\|$, $\theta_0 = \arccos(\hat{m}_z/r_0)$, and $\phi_0 = \arctan(\hat{m}_y/\hat{m}_x)$ are the spherical coordinates of the ground state $\hat{\mathbf{m}} := \text{argmin} V(\mathbf{m})$, for the potential (S49). Here $\mathbf{n}^{(dw)}$ is unit 3-vectors that encode the information about domain-walls (S60), and $\mathcal{S}^{(sk)}$ (S61) is the function that imprints skyrmions on $\mathbf{n}^{(dw)}$.

The configuration that interpolates between the north and south pole of the unit sphere can be parametrized as follow:

$$\mathbf{n}^{(dw)} = \left(\sqrt{\frac{1 - \Upsilon(\mathbf{x})^2}{2}}, \sqrt{\frac{1 - \Upsilon(\mathbf{x})^2}{2}}, \Upsilon(\mathbf{x}) \right), \quad (\text{S60a})$$

$$\Upsilon(\mathbf{x}) = \tanh\left(\frac{\mathbf{x}_\perp - \mathbf{x}_0}{\xi_{dw}}\right), \quad (\text{S60b})$$

where ξ_{dw} determines the width of the domain-wall. In (S60), \mathbf{x}_0 is the curvilinear abscissa that determines the position of the domain-wall, and \mathbf{x}_\perp is the coordinate perpendicular to the domain-wall. In the absence of domain-walls, then $\mathbf{n}^{(dw)} = (0, 0, 1)$, simply points to the north pole.

The skyrmions are implemented by successively rotating the vector $\mathbf{n}^{(dw)}$. Namely, a set of N_{sk} skyrmions is realized by successfully composing the rotations accord-

ing to

$$\mathcal{S}^{(sk)} = \prod_{k=1}^{N_{sk}} R_z(\Phi_k(\mathbf{x})) R_y(\Theta_k(\mathbf{x})). \quad (\text{S61})$$

Here again, R_i are the rotation matrices, and the angles defining a given skyrmion are

$$\Phi_k(\mathbf{x}) = Q_k \arctan\left(\frac{y - y_k}{x - x_k}\right), \quad (\text{S62a})$$

$$\Theta_k(\mathbf{x}) = \pi \exp\left\{-\frac{(x - x_k)^2 + (y - y_k)^2}{2\xi_{sk}^2}\right\}. \quad (\text{S62b})$$

The parameters (x_k, y_k) determine the position of the core of the k -th skyrmion, of charge Q_k , and ξ_{sk} determines the size of the skyrmions.

III. ADDITIONAL RESULTS

A. Skyrmions

The model has a great variety of skyrmion solutions with different different topological charges. This can be

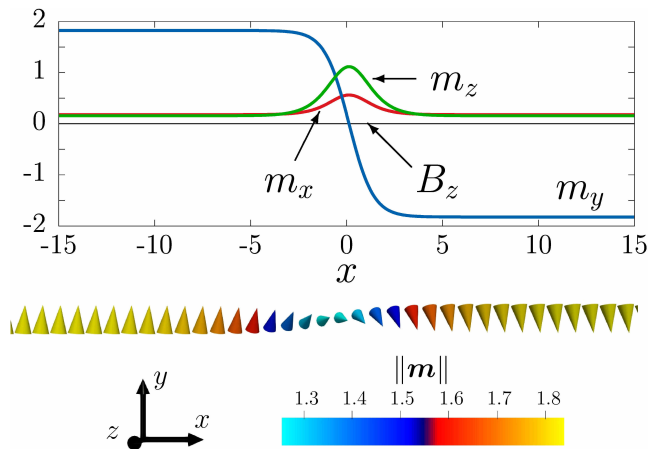


Figure S4. A domain-wall that interpolates between the inequivalent time-reversal symmetry broken states. The top panel show the different components of the fermion quadrupling order parameter \mathbf{m} . The bottom panel shows the corresponding texture. The corresponding parameters are given in Sec. IF, and the gauge coupling $e = 0.25$. The domain-walls are not associated with a magnetic field.

see from Fig. S2 that displays several examples of stable skyrmions with topological charges $\mathcal{Q}(\mathbf{m})=1-10$.

B. Skyrmions on an inhomogeneous background

The skyrmions displayed in the main body, as well as in Fig. S2, are computed in the case of completely homogeneous parameters. However, as emphasized earlier, the materials can have slight inhomogeneities in doping level. This results in relatively small modulation of T_c , and also in modulation of relative densities and phases of the gaps. As emphasized in the main body, this yields spontaneous magnetic fields. It is thus rather natural to question the effect that inhomogeneities can have on skyrmions. As already emphasized, in the considered model, the skyrmions are fairly stable objects, we find that they survive in the presence of various kinds of inhomogeneities. This can be seen from Fig. S3 that displays several examples of stable skyrmions (with topological charges $\mathcal{Q}(\mathbf{m})=2,4,7,8$), in the presence of inhomogeneities. Clearly, the skyrmions are deformed by the inhomogeneities, yet, in this case they remain robust structures. See the conclusions of the main part of the paper regarding the reservations on stability of skyrmions beyond the effective model.

C. Domain-walls

The fermion quadrupling resistive state, which precedes the $s+is$ state, spontaneously breaks the time-reversal symmetry. For the fermion quadrupling order parameter \mathbf{m} , the time-reversal operation (S55) implies that a state that breaks the time-reversal symmetry has $m_y \neq 0$. In such a situation, there exist domain-wall excitations between both $s \pm is$ states, as illustrated in Fig. S4.

* garaud.phys@gmail.com

† babaev.egor@gmail.com

- [S1] J. Garaud, M. Silaev, and E. Babaev, “Microscopically derived multi-component Ginzburg–Landau theories for $s+is$ superconducting state,” *Physica C: Superconductivity and its Applications* **533**, 63–73 (2017).
- [S2] S. Maiti and A. V. Chubukov, “ $s+is$ state with broken time-reversal symmetry in Fe-based superconductors,” *Physical Review B* **87**, 144511 (2013).
- [S3] J. Garaud, A. Corticelli, M. Silaev, and E. Babaev, “Properties of dirty two-band superconductors with repulsive interband interaction: Normal modes, length scales, vortices, and magnetic response,” *Physical Review B* **98**, 014520 (2018).
- [S4] E. Babaev, L. D. Faddeev, and A. J. Niemi, “Hidden symmetry and knot solitons in a charged two-condensate Bose system,” *Physical Review B* **65**, 100512 (2002).
- [S5] E. Babaev, “Non-Meissner electrodynamics and knotted solitons in two-component superconductors,” *Physical Review B* **79**, 104506 (2009).
- [S6] J. Garaud, K. A. H. Sellin, J. Jäykkä, and E. Babaev, “Skyrmions induced by dissipationless drag in $U(1) \times U(1)$ superconductors,” *Physical Review B* **89**, 104508 (2014).
- [S7] M. Silaev, J. Garaud, and E. Babaev, “Unconventional thermoelectric effect in superconductors that break time-reversal symmetry,” *Physical Review B* **92**, 174510 (2015).
- [S8] V. Grinenko, D. Weston, F. Caglieris, C. Wuttke, C. Hess, T. Gottschall, I. Maccari, D. Gorbunov, S. Zherlitsyn, J. Wosnitzer, A. Rydh, K. Kihou, C.-H. Lee, R. Sarkar, S. Dengre, J. Garaud, A. Charnukha, R. Hühne, K. Nielsch, B. Büchner, H.-H. Klauss, and E. Babaev, “State with spontaneously broken time-reversal symmetry above the superconducting phase transition,” *Nature Physics* **17**, 1254–1259 (2021).
- [S9] J. Garaud, M. Silaev, and E. Babaev, “Thermoelectric Signatures of Time-Reversal Symmetry Breaking States in Multiband Superconductors,” *Physical Review Letters* **116**, 097002 (2016).
- [S10] S. Maiti, M. Sigrist, and A. Chubukov, “Spontaneous currents in a superconductor with $s+is$ symmetry,”

- Physical Review B **91**, 161102 (2015).
- [S11] S.-Z. Lin, S. Maiti, and A. Chubukov, “Distinguishing between $s + id$ and $s + is$ pairing symmetries in multiband superconductors through spontaneous magnetization pattern induced by a defect,” *Physical Review B* **94**, 064519 (2016).
- [S12] V. L. Vadimov and M. A. Silaev, “Polarization of the spontaneous magnetic field and magnetic fluctuations in $s + is$ anisotropic multiband superconductors,” *Physical Review B* **98**, 104504 (2018).
- [S13] D. V. Hutton, *Fundamentals of Finite Element Analysis*, Engineering Series (McGraw-Hill, 2003).
- [S14] J. Reddy, *An Introduction to the Finite Element Method* (McGraw-Hill Education, 2005).
- [S15] F. Hecht, “New development in freefem++,” *Journal of Numerical Mathematics* **20**, 251–265 (2012), See also FreeFEM software at <https://freefem.org/>.
- [S16] R. Fletcher and C. M. Reeves, “Function minimization by conjugate gradients,” *The Computer Journal* **7**, 149–154 (1964).
- [S17] E. Polak and G. Ribière, “Note sur la convergence de directions conjuguées,” *Revue française d’informatique et de recherche opérationnelle. Série rouge* **3**, 35–43 (1969).
- [S18] B. T. Polyak, “The conjugate gradient method in extremal problems,” *USSR Computational Mathematics and Mathematical Physics* **9**, 94–112 (1969).
- [S19] J. R. Shewchuk, *An Introduction to the Conjugate Gradient Method Without the Agonizing Pain*, Tech. Rep. (Carnegie Mellon University, Pittsburgh, PA, USA, 1994).